



HAL
open science

Transcriptional profiling reveals potential involvement of microvillous TRPM5-expressing cells in viral infection of the olfactory epithelium

B. Dnate' Baxter, Eric D Larson, Laetitia Merle, Paul Feinstein, Arianna Gentile Polese, Andrew N Bubak, Christy S Niemeyer, James Hassell, Doug Shepherd, Vijay R Ramakrishnan, et al.

► To cite this version:

B. Dnate' Baxter, Eric D Larson, Laetitia Merle, Paul Feinstein, Arianna Gentile Polese, et al.. Transcriptional profiling reveals potential involvement of microvillous TRPM5-expressing cells in viral infection of the olfactory epithelium. *BMC Genomics*, 2021, 22 (1), pp.224. 10.1186/s12864-021-07528-y . hal-04581935

HAL Id: hal-04581935

<https://hal.inrae.fr/hal-04581935v1>

Submitted on 21 May 2024

HAL is a multi-disciplinary open access archive for the deposit and dissemination of scientific research documents, whether they are published or not. The documents may come from teaching and research institutions in France or abroad, or from public or private research centers.

L'archive ouverte pluridisciplinaire **HAL**, est destinée au dépôt et à la diffusion de documents scientifiques de niveau recherche, publiés ou non, émanant des établissements d'enseignement et de recherche français ou étrangers, des laboratoires publics ou privés.




Distributed under a Creative Commons Attribution 4.0 International License

RESEARCH ARTICLE

Open Access



Transcriptional profiling reveals potential involvement of microvillous TRPM5-expressing cells in viral infection of the olfactory epithelium

B. Dnate' Baxter^{1,2†}, Eric D. Larson^{3†}, Laetitia Merle^{1,2†}, Paul Feinstein⁴, Arianna Gentile Polese^{1,2}, Andrew N. Bubak⁵, Christy S. Niemeyer⁵, James Hassell Jr⁵, Doug Shepherd⁶, Vijay R. Ramakrishnan³, Maria A. Nagel⁵ and Diego Restrepo^{1,2*} 

Abstract

Background: Understanding viral infection of the olfactory epithelium is essential because the olfactory nerve is an important route of entry for viruses to the central nervous system. Specialized chemosensory epithelial cells that express the transient receptor potential cation channel subfamily M member 5 (TRPM5) are found throughout the airways and intestinal epithelium and are involved in responses to viral infection.

Results: Herein we performed deep transcriptional profiling of olfactory epithelial cells sorted by flow cytometry based on the expression of mCherry as a marker for olfactory sensory neurons and for eGFP in OMP-H2B:mCherry/TRPM5-eGFP transgenic mice (*Mus musculus*). We find profuse expression of transcripts involved in inflammation, immunity and viral infection in TRPM5-expressing microvillous cells compared to olfactory sensory neurons.

Conclusion: Our study provides new insights into a potential role for TRPM5-expressing microvillous cells in viral infection of the olfactory epithelium. We find that, as found for solitary chemosensory cells (SCCs) and brush cells in the airway epithelium, and for tuft cells in the intestine, the transcriptome of TRPM5-expressing microvillous cells indicates that they are likely involved in the inflammatory response elicited by viral infection of the olfactory epithelium.

Keywords: Olfactory sensory neurons, Microvillous cells, Viral infection, Immunity, Inflammation, Mouse

* Correspondence: diego.restrepo@cuanschutz.edu

B. Dnate' Baxter, Eric D. Larson and Laetitia Merle are Co-first authors.

¹Neuroscience Graduate Program, University of Colorado Anschutz Medical Campus, Aurora, CO 80045, USA

²Department of Cell and Developmental Biology, University of Colorado Anschutz Medical Campus, Aurora, CO 80045, USA

Full list of author information is available at the end of the article



© The Author(s). 2021 **Open Access** This article is licensed under a Creative Commons Attribution 4.0 International License, which permits use, sharing, adaptation, distribution and reproduction in any medium or format, as long as you give appropriate credit to the original author(s) and the source, provide a link to the Creative Commons licence, and indicate if changes were made. The images or other third party material in this article are included in the article's Creative Commons licence, unless indicated otherwise in a credit line to the material. If material is not included in the article's Creative Commons licence and your intended use is not permitted by statutory regulation or exceeds the permitted use, you will need to obtain permission directly from the copyright holder. To view a copy of this licence, visit <http://creativecommons.org/licenses/by/4.0/>. The Creative Commons Public Domain Dedication waiver (<http://creativecommons.org/publicdomain/zero/1.0/>) applies to the data made available in this article, unless otherwise stated in a credit line to the data.

Background

Chemosensory cells found in the airway (SCCs/brush cells) and intestinal epithelium (tuft cells) express the transient receptor potential cation channel subfamily M member 5 (TRPM5) and other elements of the taste transduction pathway and have been implicated in immune and inflammatory responses to bacterial, viral and parasitic infection [53, 54, 62, 68, 73, 75, 85]. In the olfactory epithelium TRPM5 and other proteins involved in taste transduction are also expressed in SCC-like microvillous cells (MVCs) [28, 48], which have been proposed to be involved in a protective response to high concentrations of odorants [25, 42]. However, whether MVCs play a role in viral infection or viral infection defense of the olfactory epithelium is unknown.

Herein, we performed transcriptional profiling of MVCs and a subset of olfactory sensory neurons (OSNs) expressing eGFP under control of a fragment of the TRPM5 promoter (OSN_eGFP+ cells) [49, 50]. In order to profile these low abundance cells we performed transcriptional profiling of specific cell types sorted by fluorescence-activated cell sorting (FACS). We crossed a mouse expressing mCherry in the nuclei of OSNs under control of the OMP promoter (OMP-H2B::mCherry mice) with TRPM5-eGFP transgenic mice [14] (OMP-H2B::mCherry/TRPM5-eGFP mice). We isolated cells from the olfactory epithelium and used FACS to sort MVC_eGFP cells (mCherry negative and eGFP positive) and cells labeled by OMP-driven mCherry that did or did not express eGFP (OSN_eGFP+ and OSN_eGFP- cells) followed by transcriptional profiling by RNA sequencing (RNAseq).

Results

Fluorescence-activated cell sorting of cells isolated from the main olfactory epithelium

The olfactory epithelium of OMP-H2B::mCherry/TRPM5-eGFP mice expressed nuclear mCherry driven by the OMP promoter in the intermediate layer of the olfactory epithelium (Fig. 1a), as expected for the location of nuclei of mature OSNs [22]. eGFP expression driven by the TRPM5 promoter was found in MVCs, with cell bodies located mostly in the apical layer of the epithelium (asterisks), and at lower expression levels in a subset of OSNs double-labeled with mCherry (Fig. 1a), consistent with earlier publications [48, 49].

We proceeded to isolate cells from the main olfactory epithelium of OMP-H2B::mCherry/TRPM5-eGFP mice (see Fig. 1b, Methods, Table 1 and Figure 1 - figure supplement 1). Figure 1c shows two isolated OSNs with differential expression of eGFP. Using flow cytometry we found that fluorescence intensity of individual cells for mCherry and eGFP spanned several orders of magnitude (Fig. 1d). We proceeded to sort three groups of cells

under light scattering settings to exclude doublets: high mCherry-expressing cells with low and high eGFP fluorescence (presumably mature OSNs, these cells are termed OSN_eGFP- and OSN_eGFP+ cells respectively) and cells with low mCherry and high eGFP expression (MVC_eGFP, presumably MVCs). Reverse transcription quantitative PCR (RT-qPCR) showed that, as expected the OSN_eGFP- and OSN_eGFP+ cells have higher levels of OMP transcript than MVC_eGFP cells (Fig. 1e, i), and OSN_eGFP+ cells and MVC_eGFP cells have higher levels of eGFP transcript compared to OSN_eGFP- cells (Fig. 1e,ii). Furthermore, compared to OSN_eGFP- cells both the MVC_eGFP cells and OSN_eGFP+ cells expressed higher levels of TRPM5 transcript (Fig. 1e,iii) and choline acetyl transferase (ChAT)(Fig. 1e,iv), a protein involved in acetylcholine neurotransmission that is expressed in MVCs [63]. The asterisks in Fig. 1e denote significant differences tested with either t-test or ranksum with *p*-values below the *p*-value of significance corrected for multiple comparisons using the false discovery rate (pFDR) [15] (pFDR is 0.033 for OMP, 0.05 for TRPM5, 0.05 for EGFP and 0.03 for ChAT, *n* = 8 for OMP OSN_eGFP-, 4 for OMP OSN_eGFP+ and 4 for MVC_eGFP cells).

RNAseq indicates that MVC_eGFP and OSN_eGFP- are distinct groups of chemosensory cells in the mouse olfactory epithelium

Differential gene expression analysis of the RNAseq data was used to compare MVC_eGFP and OSN_eGFP- sorted by FACS. Expression of 4386 genes was significantly higher in MVC_eGFP cells compared to OSN_eGFP- cells, and expression of 5630 genes was lower in MVC_eGFP cells (Fig. 2a shows the most significantly upregulated or downregulated genes and Figure 2 - figure supplement 1 shows the entire list). A total of 1073 Olf genes were included in the analysis (including pseudogenes). While 9 were expressed at higher levels in the MVC_eGFP population their expression levels was very low (<100 counts) and the difference was not statistically significant. On the contrary, transcripts for 550 olfactory receptors were significantly higher in OSN_eGFP- cells (Fig. 2b and c). *Trpm5* and *eGFP* were among the top 10 genes whose transcription was higher in MVC_eGFP cells compared to OSN_eGFP- cells with 1471-fold and 75-fold differences respectively (Fig. 2a). Interestingly, *Pou2f3*, a transcription factor important in differentiation of MVCs [92, 93], is found within the top 10 upregulated genes found in MVC_eGFP cells compared to OSN_eGFP- (Fig. 2a). In addition, transcripts for chemosensory cell specific cytokine IL-25 and its receptor IL-17RB [86] were more highly expressed in MVC_eGFP (Figure 2 - figure supplement 1). Finally, *OMP* and *s100a5*, genes for two proteins expressed in

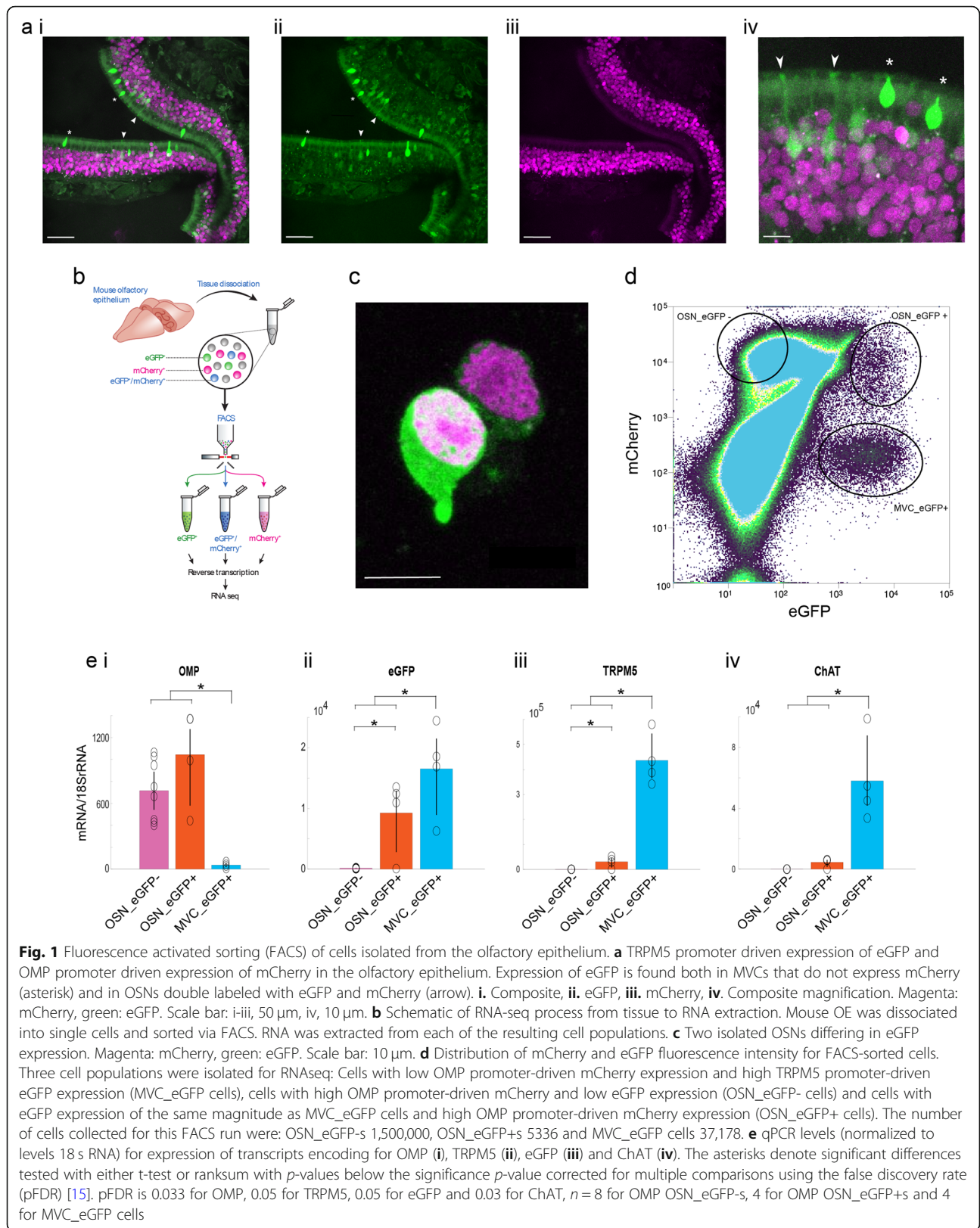


Table 1 List of key resources and reagents used in this study

REAGENT TYPE	REAGENT or RESOURCE	SOURCE	IDENTIFIER	ADDITIONAL INFORMATION
Chemical compound, drug	BrainPhys Neuronal Medium	Stemcell Technologies		Product # 05791
Chemical compound, drug	Dispase II	Sigma		Product # D4693
Chemical compound, drug	AcGFP1/eGFP calibration beads	Takara		Flow cytometry calibration beads Product # 632594
Chemical compound, drug	mCherry calibration beads	Takara		Flow cytometry calibration beads Product # 632595
Chemical compound, drug	RQ1 RNase-free DNase	Promega		Product # M6101
Chemical compound, drug	Papain	Sigma		Product # P3125
Chemical compound, drug	Paraformaldehyde (32%)	Electron Microscopy Sciences		Product # 157145
Chemical compound, drug	RNAprotect Tissue Reagent	Qiagen		Product # 76526
Chemical compound, drug	RNeasy Plus Micro Kit	Qiagen		Product # 74034
Chemical compound, drug	High Capacity c-DNA Reverse Transcription kit	ABI		
Chemical compound, drug	18 s rRNA	PE ABI		
Strain, strain background	TRPM5-eGFP	Dr. Robert Margolskee [14]		
Strain, strain background	TRPM5 knockout	Dr. Robert Margolskee [16]		
Strain, strain background	OMP-H2B::Cherry	Generated for this publication		This mouse will be deposited in Jackson Laboratories
Software, algorithm	MATLAB_R2018a	Mathworks	RRID: SCR_001622	
Software, algorithm	Illustrator	Adobe	RRID: SCR_010279	
Software, algorithm	Photoshop	Adobe	RRID: SCR_014199	
Software, algorithm	InDesign	Adobe		
Software, algorithm	MoFlo Astrios Summit Software (6.3.1.16945).	Beckman Coulter		
Software, algorithm	BBMap (BBDuk)		RRID:SCR_016968	
Software, algorithm	Salmon v1.2.1	https://combine-lab.github.io/salmon/	RRID:SCR_017036	[67]
Software, algorithm	DeSEQ2 v1.28.0	bioconductor.org https://bioconductor.org/packages/release/bioc/html/DESeq2.html	RRID:SCR_015687	[51]
Software, algorithm	TopGO, v2.40.0		RRID:SCR_014798	
Software, algorithm	pHeatmap, 1.0.12		RRID:SCR_016418	
Software, algorithm	Ensembl GRCm38, v99			
Software, algorithm	R, v4.0		RRID:SCR_001905	
Software,	Tximport, v1.16.0		RRID:SCR_	

Table 1 List of key resources and reagents used in this study (Continued)

REAGENT TYPE	REAGENT or RESOURCE	SOURCE	IDENTIFIER	ADDITIONAL INFORMATION
algorithm			016752	
Software, algorithm	SAMtools	SAMtools http://samtools.sourceforge.net/	RRID:SCR_002105	[44]
Software, algorithm	Bedtools		RRID:SCR_006646	
Software, algorithm	STAR v2.5.3a	https://github.com/alexdobin/STAR	RRID:SCR_015899	
Software, algorithm	Sigmaplot, v12.5	Systat Software	RRID:SCR_003210	
Software, algorithm	Custom code for bioinformatics analysis	https://github.com/eric-d-larson/OE_TRPM5		
Software, algorithm	OPM	https://github.com/qi2lab/opm		

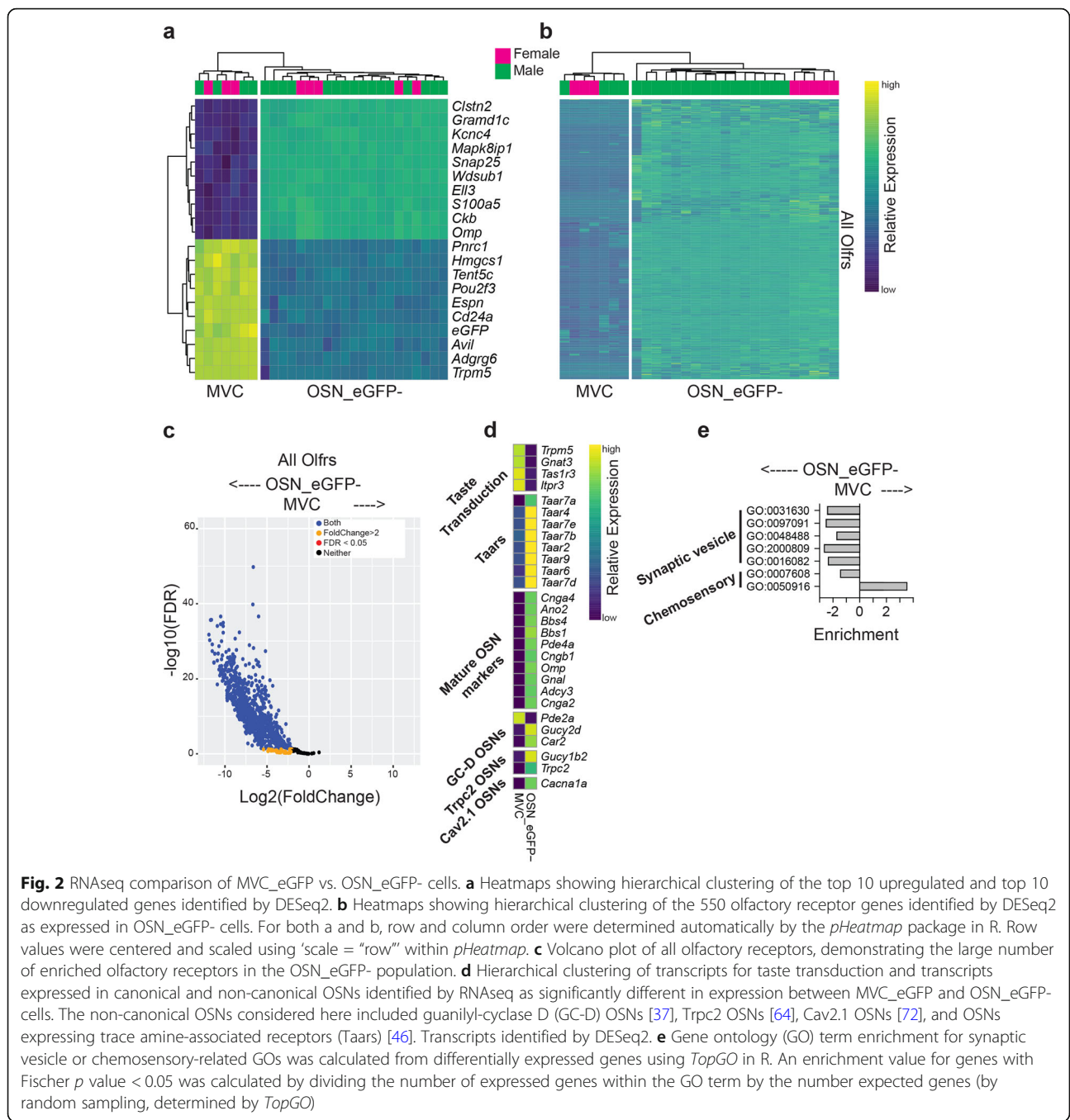
mature OSNs [22, 23], were among the top 10 downregulated transcripts in MVC_eGFP cells compared to OSN_eGFP- cells (Fig. 2a).

We compared expression of transcripts involved in taste transduction, canonical olfactory transduction, and non-canonical OSNs (Fig. 2d). MVC_eGFP cells expressed genes involved in the taste transduction pathway as expected for chemosensory epithelial cells of the olfactory epithelium [86]. In contrast, OSN_eGFP-expressed transcripts for markers of canonical OSNs such as OMP, BBS1 and 2 and proteins involved in the canonical olfactory transduction pathway. The non-canonical OSNs considered here included guanylyl-cyclase D (GC-D) OSNs [37], *Trpc2* OSNs [64] and *Cav2.1* OSNs [72]. OSN_eGFP- expressed low levels of *Cacna1a* encoding for *Cav2.1* and *Trpc2*. OSN_eGFP-expressed higher levels of Trace amine-associated receptors [46] than MVC_eGFP cells.

Perusal of these top differences suggested that these are distinct chemosensory cell types found in the olfactory epithelium. In order to perform a thorough analysis of the differences between these chemosensory cell groups we performed an analysis of gene ontology (GO) enrichment for lists of genes related to chemosensory perception and neuronal identity. When compared with OSN_eGFP- we found that MVC_eGFP cells express higher levels of transcripts belonging to gene ontologies of sensory perception of sweet/umami taste (GO: 0050916 and GO:0050917) (Fig. 2e, Figure 2 - figure supplement 2, Figure 2 - figure supplement 3) which includes taste detection/transduction proteins that have been reported to be expressed in MVCs [28, 34]: *Gnat3*, encoding for gustducin, the G protein mediating sweet and umami taste transduction [56], *Itpr3*, encoding for the inositol-1,4,5-triphosphate receptor type 3 and *Tas1r3*, encoding for a gustducin-coupled receptor involved in umami and sweet taste [17, 99]. In contrast, OSN_eGFP- express at higher levels than MVCs

transcripts involved in events required for an organism to receive an olfactory stimulus, convert it to a molecular signal, and recognize and characterize the signal (GO:0007608). Finally, enrichment of gene ontology lists for synaptic vesicle function were decreased for MVC_eGFP cells compared with OSN_eGFP- cells (Fig. 2e). Results of this gene ontology analysis of chemosensation and synaptic vesicle function reinforces the finding that the two cell groups in this study are distinct chemosensory cell types of the olfactory epithelium. OSN_eGFP-cells differ from MVC_eGFP cells in expression of olfactory receptors, chemosensation and transcripts related to synaptic function as expected for an OSN.

Finally, a question that arises is how the transcriptional profile of the MVC_eGFP cells of this study compares to transcriptional profiling of chemosensory epithelial cells isolated from the respiratory and olfactory epithelia in mice expressing eGFP under control of the ChAT promoter [86]. Figure 2 - figure supplement 4 shows comparisons of gene expression between MVC_eGFP and OSN_eGFP- cells of this study and ChAT-eGFP MVCs and ChAT-eGFP SCCs profiled in the respiratory epithelium in the study of Ualiyeva and co-workers [86]. This comparison is of limited value due to the fact that gene profiling was performed in two separate studies. However, in this preliminary analysis we find that MVCs from this study have similar transcription profiles to ChAT-eGFP MVCs and differ from ChAT-eGFP SCCs. For example, MVC_eGFP and ChAT-eGFP MVCs showed enhanced expression of transcripts such as *Il25* and *Fos* (Figure 2 - figure supplement 3). The similarity of transcriptional profiling argues that in this study MVC_eGFPs were not contaminated with SCCs consistent with the fact that in our study we isolated MVC_eGFP from olfactory epithelium dissected apart from the respiratory epithelium and that the density of MVCs in the OE is higher than the density of SCCs in the respiratory epithelium [86] decreasing the chance of



contamination of OE MVCs by SCCs. Interestingly, *Ugt2a1* and *Ugt2a2*, transcripts for proteins involved in UDP synthesis were higher in MVC_eGFP than ChAT-eGFP MVCs suggesting differences between these cells (Figure 2 - figure supplement 3). In order to determine whether these similarities and differences between MVCs in our study and the study of Ualiyeva and co-workers are real it will be necessary to perform simultaneous RNAseq profiling of these two populations.

Gene ontology analysis finds enrichment of lists of viral-related, inflammation and immune transcripts in MVC_eGFP cells

SCCs, tuft and brush cells have been implicated in responses to bacterial and viral infection, immunity and inflammation [53, 54, 62, 68, 73, 75, 85, 86]. The fact that MVCs are closely related to these cells [25, 28, 63, 86] lead us to search for gene ontology enrichment related to bacterial and viral infection, immunity and inflammation for MVC_eGFP cells. We found robust

enrichment of these gene ontologies in MVC_eGFP cells (Fig. 3a). Transcripts related to viral infection that were higher in MVC_eGFP cells compared to OSN_eGFP-cells (Fig. 3b) included those involved in viral entry into host cells, viral transcription and regulation of viral transcription, negative regulation of viral genome replication and negative regulation of viral process (Figure 2 – figure supplement 2). The majority of these genes were detected by Ualiyeva and colleagues [86] in their ChAT-GFP MVC population. We also found gene ontology enrichment in MVC_eGFP cells compared to OSN_eGFP-cells for defense response to bacterium (Figure 2 – figure supplement 2).

Importantly, we also find enrichment for transcript expression for immunity and inflammation. Genes related to inflammation and immunity that were higher in MVC_eGFP cells compared to OSN_eGFP- cells are shown in Figure 3 – figure supplements 1–2. Among these transcripts *IL25* and its receptor *Il17rb* are found

at higher levels in MVC_eGFP cells. In SCCs, brush cells and tuft cell generation of IL25 leads to a type 2 inflammation and stimulates chemosensory cell expansion in a sequence of events that also involves cysteinyl leukotrienes [4, 53, 90]. The presence of both *Il25* and *Il17rb* suggests an autocrine effect. Furthermore, both cell types displayed increased expression of transcripts encoding for enzymes involved in eicosanoid biosynthesis such as *Alox5*, *Ptgs1* and *Ptgs2* that are found in brush cells in the airways [4] and tuft cells in the intestine [55] where they drive type 2 immune responses.

Transcription profiling suggest that OSN_eGFP+ cells are distinct from both OSN_eGFP- and MVC_eGFP cells

Differential gene expression analysis of the RNAseq data was used to compare OSN_eGFP+ individually with the other two groups of cells. We found that expression of 2000 genes was significantly higher in OSN_eGFP+ compared to OSN_eGFP-, and expression of 1821 genes

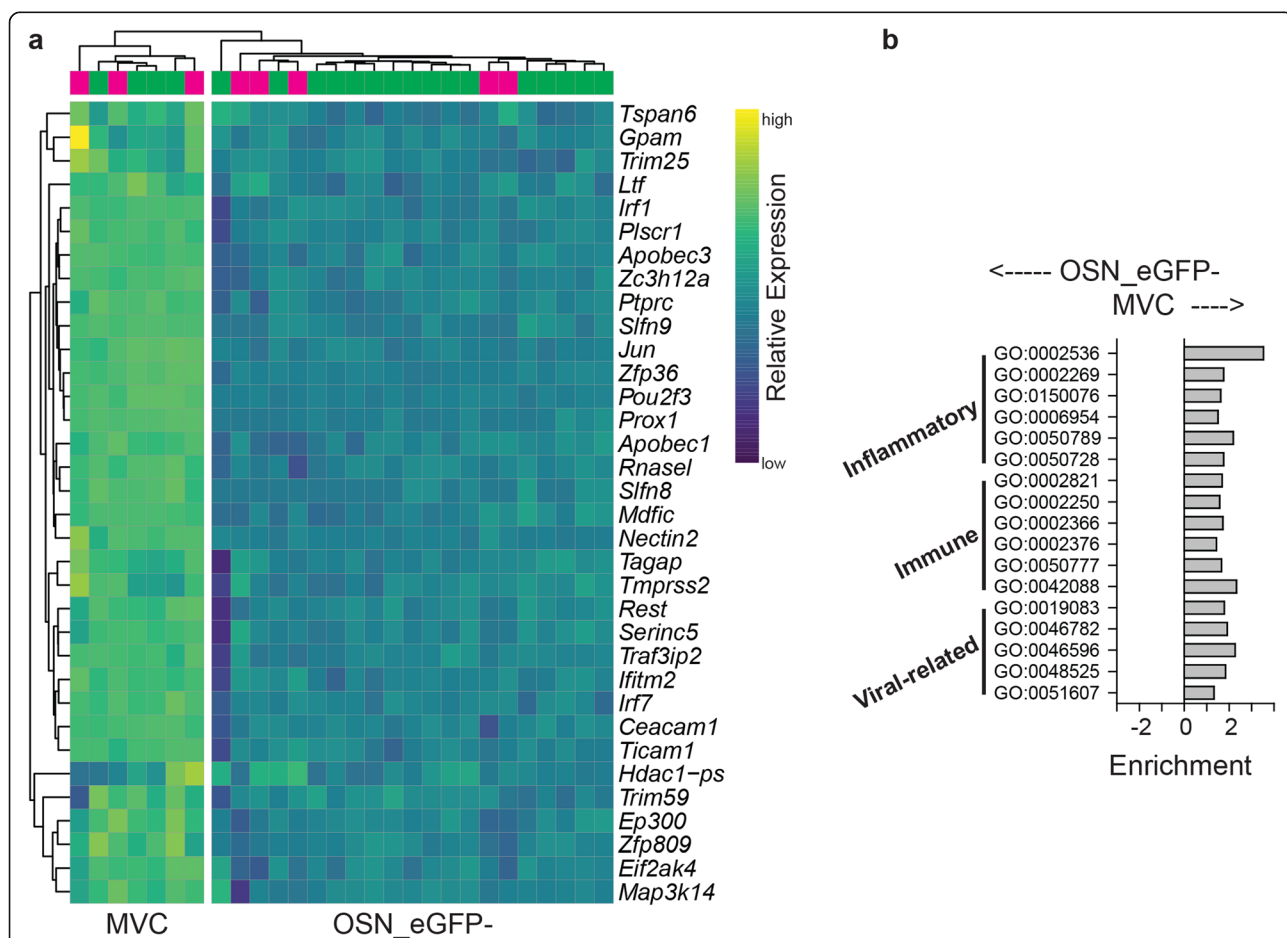


Fig. 3 Significant differences in virally-related, immune and inflammation gene ontology lists between MVC_eGFP and OSN_eGFP-. **a** Gene ontology (GO) term enrichment was calculated from differentially expressed genes using TopGO in R for OSN_eGFP- vs. MVC_eGFP cells. An enrichment value for genes with Fischer *p* value < 0.05 was calculated by dividing the number of expressed genes within the GO term by the number expected genes (by random sampling, determined by TopGO). Heatmap show hierarchical clustering of significantly differentially expressed genes identified by DESeq2. **b** Significant differences in virally-related genes within the MVC_eGFP cells compared to OSN_eGFP-

was lower in OSN_eGFP+ cells (Figure 4 -figure supplement 1 shows the results of RNAseq and Figure 4 -figure supplement 2 summarizes the data). Figure 4 figure supplement 2a shows expression levels for the transcripts that showed the largest differences between OSN_eGFP+ and OSN_eGFP- cells. The transcripts for TRPM5 and eGFP were among the top 10 genes whose transcription was higher in OSN_eGFP+ compared to OSN_eGFP- with 105-fold and 42-fold increases respectively. However all of these 10 top genes, and many other genes that were found at significantly higher levels of expression in OSN_eGFP+ cells compared to OSN_eGFP- happen to be genes expressed at significantly higher levels in MVC_eGFP cells (Figure 4 -figure supplement 3 shows the results of RNAseq for MVC_eGFP vs OSN_eGFP+). For example *Trpm5* is expressed at levels of 87.5, 9200 and 127,000 in OSN_eGFP-, OSN_eGFP+ and MVC_eGFP cells respectively (Figure 4 -figure supplement 4). While the light scatter settings in the FACS were set to exclude doublets, this raised the question whether expression of these genes in the OSN_eGFP+ pool was due to contamination of the OSN_eGFP+ cell fraction (mCherry and eGFP positive) by doublets made up of one OSN_eGFP- cell (mCherry positive and eGFP negative) and one MVC_eGFP cell (mCherry negative and GFP positive).

In order to determine whether transcription profiling for the OSN_eGFP+ cell fraction is consistent with this being a separate population we searched for genes whose expression levels were significantly higher in OSN_eGFP+ compared to *both* OSN_eGFP- and MVC_eGFP. Figure 4a and b show the top genes that were expressed at significantly higher levels in OSN_eGFP+ (and Figure 4 - figure supplement 5 shows data for all 80 genes). Among these genes there were 22 olfactory receptor genes (Table 2) and one olfactory receptor pseudogene (Fig. 4b, c shows a volcano plot for *Olfrs*). Many of these olfactory receptors were linked within the same *Olf* cluster (e.g. *olfr727* and *olfr728*; *olfr390* and *olfr391*; *Olf* 292-*Olf*307). In particular, *Olf*727 and *Olf*728 are amongst the top 6 expressed *Olf*rs in the entire olfactory epithelium and their greater representation within OSN_eGFP+ cells, suggests a functional contribution. A GOnet GO term enrichment analysis [70] of the 80 genes expressed at higher levels in OSN_eGFP+ compared to the other two groups (Figure 4 - figure supplement 6) indicated that these cells express genes involved in sensory perception of smell (GO:0007608), signal transduction (GO:0007165) and cellular response to stimulus (GO:0051716). Interestingly, two of these genes *Trpc2* [64] and *Calb2* [5] are expressed in small subsets of OSNs. Thus, this analysis suggests that OSN_eGFP+ cells are distinct from the other two cell populations, although more detailed follow-up experiments with orthogonal methods such as in situ,

immunohistochemistry and single cell RNA sequencing are necessary to fully characterize this population. Our data do not provide conclusive evidence for the existence of a distinct population of OSN_eGFP+ cells.

Gender differences for expression of olfactory receptors

We did not find major differences in transcriptome profiling between males and females for genes that were differentially expressed between the three cell groups (Figure 4 - figure supplement 7, 8). We found a substantial number of olfactory receptor genes that were differentially expressed between males and females (Figure 4 - figure supplement 8). Interestingly, *Trpc2*, that is one of the genes with higher expression in OSN_eGFP+ cells is expressed in higher amounts in females. Surprisingly, the differentially expressed olfactory receptors differed from receptors identified by van der Linden et al. [88].

In situ hybridization chain reaction finds strong TRPM5 mRNA expression in MVC_eGFP cells, but not in the nuclear OSN layer

Studies with regular in situ hybridization find expression of TRPM5 mRNA in MVCs, but not in the OSN nuclear layer [71, 92]. Here we asked whether third generation in situ hybridization chain reaction version 3.0 (HCR v3.0) designed to provide high signal to noise ratio in situ signal [13] revealed TRPM5 mRNA expression in the nuclear OSN layer. These experiments were performed in TRPM5-GFP mice and in TRPM5-GFP mice crossed with TRPM5 knockouts [14, 16]. Consistent with published results [71, 92] we find strong in situ signal for TRPM5 in MVC_eGFP cells located in the apical layer of the olfactory epithelium (Fig. 5a, asterisks, also see Figure 5 - figure supplement 1 for a 3D rendering) and this signal is absent in MVC_eGFP cells in the TRPM5 knockout (Fig. 5b, asterisks). In addition, we find sparse TRPM5 in situ labeling in the nuclear OSN layer (Fig. 5a, arrows), but similar sparse labeling was found in the OSN nuclear layer in the TRPM5 knockout (Fig. 5b, arrows). Therefore, we find evidence for strong expression of TRPM5 mRNA in MVC_eGFP cells, but cannot find conclusive evidence by in situ for expression of TRPM5 mRNA in OSNs.

Discussion

We performed transcriptional profiling of three chemosensory cells in the mouse olfactory epithelium: microvillous cells (MVC_eGFP) and two types of olfactory sensory neurons: OSN_eGFP+ and OSN_eGFP-. We found that while the transcriptome of each of these cell types is distinct they share common features across groups. The two groups of OSNs share transcript

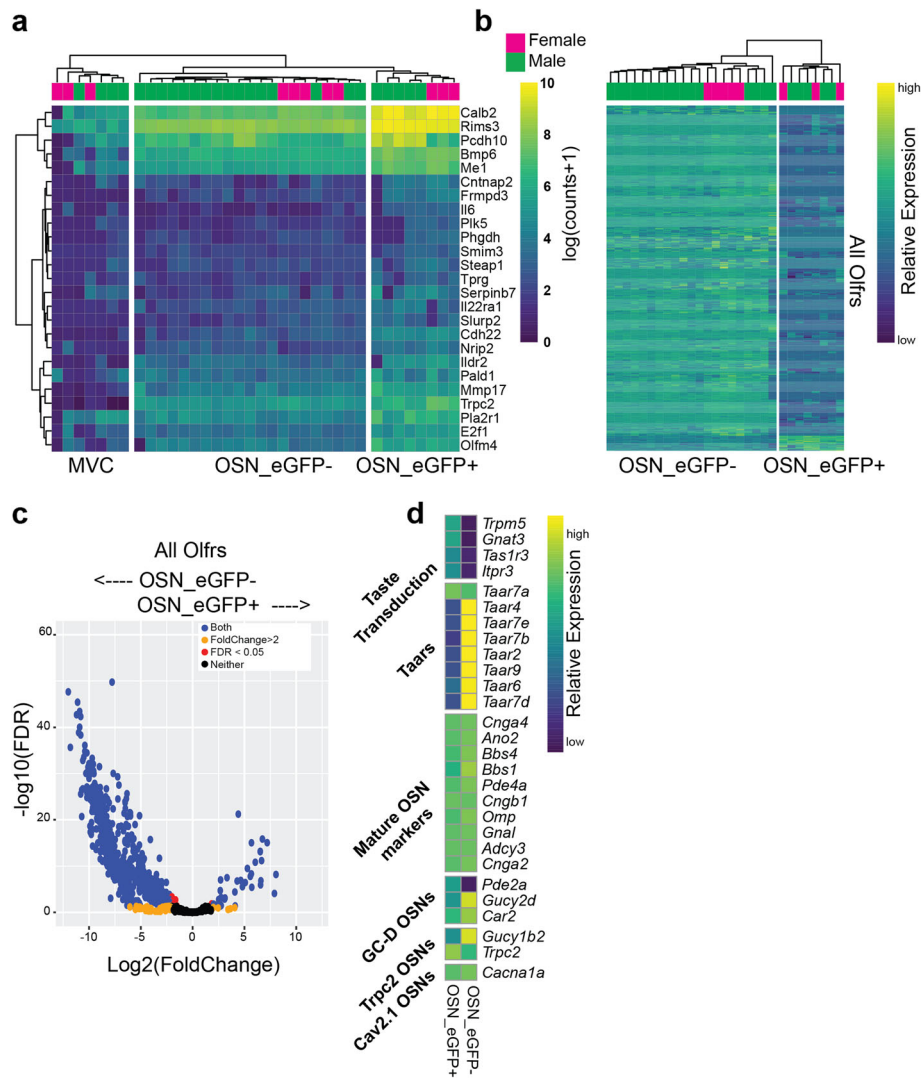


Fig. 4 RNAseq comparison of OSN_eGFP+ to both MVC_eGFP and OSN_eGFP- cells. **a** Heatmap showing the top upregulated genes (excluding Olfirs) that are expressed in OSN_eGFP+ cells 4 fold higher than OSN_eGFP- AND MVC_eGFP cells. Additional criteria for inclusion was mean of expression > standard deviation of expression and mean of expression greater than 100. **b** Heatmap showing all *Olfir* genes differentially expressed between OSN_eGFP+ and OSN_eGFP- cells identified by DESeq2. MVC_eGFP cells did not express Olfirs. For both a and b, row and column order were determined automatically by the *pHeatmap* package in R. For each data point relative expression was calculated by subtracting the average row value from each individual value. **c** Volcano plot of all Olfactory receptors, demonstrating the small number of enriched olfactory receptors in the OSN_eGFP+ population. **d** Hierarchical clustering of transcripts for taste transduction and transcripts expressed in canonical and non-canonical OSNs identified by RNAseq as significantly different in expression between the cell groups. We compared expression of transcripts involved in taste transduction, canonical olfactory transduction, and non-canonical OSNs. The non-canonical OSNs considered here included guanylyl-cyclase D (GC-D) OSNs [37], Trpc2 OSNs [64], Cav2.1 OSNs [72], and OSNs expressing trace amine-associated receptors (Taars) [46]. Transcripts identified by DESeq2

expression for proteins expressed in OSNs such as OMP, olfactory transduction proteins, and proteins involved in synaptic function. Yet, they differ in olfactory receptor expression and OSN_eGFP+ express transcripts encoding for proteins involved in chemosensory signal transduction and cellular response to stimulus. However, we did not validate the OSN_eGFP+ population using orthogonal methods and whether they are a distinct OSN population is an

open question. On the other hand, MVC_eGFP cells express transcripts encoding for taste transduction proteins and other transcripts found in SCCs such as *Pou2f3* and *Il25* but they do not express transcripts for proteins involved in olfactory transduction and synaptic function, and they do not express olfactory receptors. Finally, we found that MVC_eGFP cells express a substantial number of transcripts involved in viral infection, inflammation and immunity.

Table 2 Levels of expression and adjusted *p*-value for the olfactory receptor genes whose levels are significantly higher in OSN_eGFP+ compared to OSN_eGFP-. These olfactory receptors had an adjusted *p*-value for expression level difference between OSN_eGFP+ compared to OSN_eGFP- and had a fold change > 4 and average expression > 100 counts

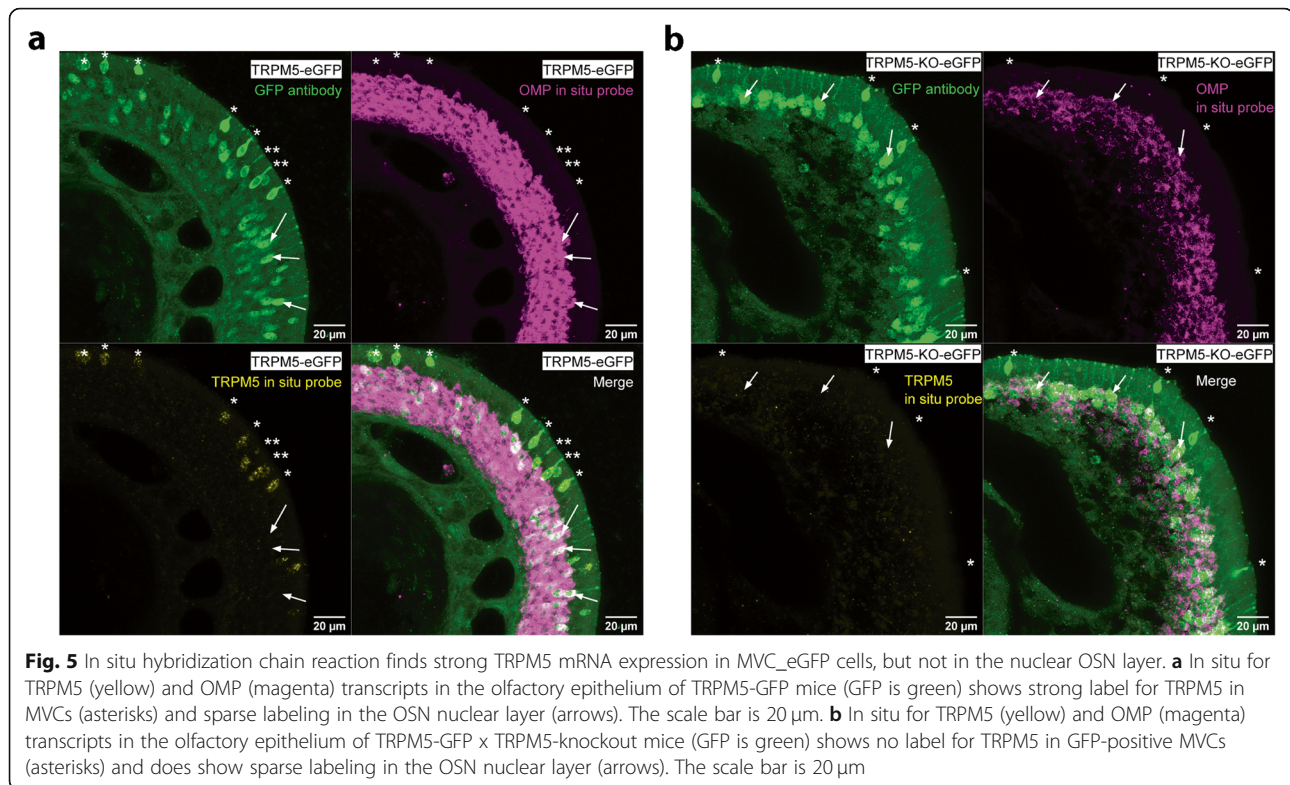
Name	OSN_eGFP-	OSN_eGFP+	MVC_eGFP	<i>p</i> -value adjusted
<i>Olfir292</i>	3.61	959	4.29	6.35E-09
<i>Olfir282</i>	2.05	486	0	8.01E-05
<i>Olfir1434</i>	53.3	7730	0	9.71E-16
<i>Olfir390</i>	101	10800	43.1	1.56E-16
<i>Olfir305</i>	6.14	612	0	6.3E-12
<i>Olfir293</i>	6.96	664	16.9	1.42E-07
<i>Olfir378</i>	3.41	322	0	1.1E-06
<i>Olfir128</i>	39.6	3660	12.7	7.33E-14
<i>Olfir344</i>	16.2	1050	0	1.4E-11
<i>Olfir307</i>	7.59	393	0	3.76E-06
<i>Olfir391</i>	156	8000	9.79	1.01E-15
<i>Olfir299</i>	13.1	651	0	4.58E-09
<i>Olfir142</i>	36.4	1720	3.77	1.62E-08
<i>Olfir1</i>	147	5720	52.7	3.08E-10
<i>Olfir1279</i>	16.4	552	10.9	3.52E-07
<i>Olfir39</i>	13.8	388	21	2.81E-06
<i>Olfir1447</i>	64.1	1610	0	1.23E-07
<i>Olfir728</i>	2150	45,700	320	6.13E-22
<i>Olfir727</i>	560	11,000	179	1.64E-07
<i>Olfir1555-ps1</i>	10.1	175	0	0.0397
<i>Olfir346</i>	27.6	465	0	3.85E-05
<i>Olfir1228</i>	533	5320	35.4	3.09E-08
<i>Olfir1181</i>	87.4	766	4.61	0.000766
<i>Olfir943</i>	97.1	844	2.89	0.000886
<i>Olfir298</i>	60.1	509	0	0.00132

Transcriptional profiling reveals a role of microvillous cells in viral infection and innate immunity

Gene ontology analysis revealed that MVC_eGFP cells express viral-related transcripts at significantly higher levels than OSN_eGFP- cells (Fig. 3 and Figure 2 – figure supplement 2). GOnet GO term enrichment analysis [70] of all 133 immune genes expressed at higher levels in MVC_eGFP cells compared to OSN_eGFP- (Figure 3 – figure supplement 2) revealed that MVCs express a substantial number of genes involved in the innate immune response (GO:0045087, 72 genes matched this list). Figure 6 depicts several mechanisms that could occur in MVC_eGFP in response to viral infection. To infect cells, viruses must interact with host cell membranes to trigger membrane fusion and viral entry. Membrane proteins at the surface of the host cell are

thus key elements promoting or preventing viral infection. Here we find that transcripts for several membrane proteins and cell adhesion molecules involved in viral entry are expressed at higher levels in MVC_eGFP cells compared to OSN_eGFP- cells. *Plscr1* encodes a phospholipid scramblase which has been shown to promote herpes simplex virus (HSV) entry in human cervical or vaginal epithelial cells and keratinocytes [12], and hepatitis C virus entry into hepatocytes [32]. In contrast with its role in viral entry, PLSCR1 impairs the replication of other types of viruses in infected cells (influenza A virus [52], hepatitis B virus [96]). IFITM2 is another transmembrane protein that mediates viral entry. In contrast with PLSCR1, IFITM2 inhibits viral entry of human immunodeficiency virus (HIV [97]), hepatitis C virus [60], influenza A H1N1 virus, West Nile virus, and dengue virus [8]. IFITM2 also inhibits viral replication [8] and protein synthesis [41]. Nectins are transmembrane glycoproteins and constitute cell surface receptors for numerous viruses. There is wide evidence that HSV can enter host cells through Nectin-1 dependent mechanisms, particularly for neuronal entry [40, 69, 76, 79], and Nectin-4 appears essential for measles virus epithelial entry [61, 80, 81]. In addition to cell surface molecules, the mucus contains secreted proteins that confer protection against viruses to the underlying cells. Glycoproteins are major constituents of mucus and exhibit multiple pathogens binding-sites. We found the *Ltf* transcript in MVC_eGFP cells, which encodes for lactotransferrin. Lactotransferrin is a globular glycoprotein widely represented in the nasal mucus with antiviral activity against Epstein-Barr virus [100, 101], HSV [78, 87] and Hepatitis C virus [2]. Finally, MVC_eGFP cells express the murine norovirus (MNoV) receptor CD300LF. In the gut TRPM5-expressing tuft cells express high levels of CD300LF and mice were resistant to infection with MNoV^{CR6} when tuft cells were absent or decreased, whereas viral titers were enhanced in any context where tuft cell numbers were increased, such as helminth infection or treatment with rIL-25 [91].

Viruses have developed numerous strategies to overcome barrier mechanisms to enter the cells. After viral entry infected cells have other resources to fight against viral infection by disrupting the production of new viral particles, limiting inflammation processes and activating innate immune responses. For example, TRIM25, whose transcript is increased in MVC_eGFP cells, is an ubiquitin ligase that activates retinoic acid-inducible gene I (RIG-I) to promote the antiviral interferon response [27]. Furthermore, influenza A virus targets TRIM25 to evade recognition by the host cell [26]. In addition, TRIM25 displays a nuclear role in restricting influenza A virus replication [57]. Zc3h12a, also known as MCP1-1, inhibits hepatitis B and C virus replication,



reduces virus-induced inflammation [45, 47], and exerts antiviral effects against influenza A virus [19].

We show that MVC_eGFP express *Gnat3*, *Plcg2* and *Itp3*. This intracellular pathway would lead to calcium increase and opening of TRPM5, leading to a sodium influx and potential vesicle release. Among the list of inflammation genes found at significantly higher levels in MVC_eGFP compared to OSN_eGFP- cells we find *Il25*, an interleukin that is involved in the type 2 inflammatory response of TRPM5-expressing epithelial cells in the airway epithelium and the gut [62, 84]. Also, *Il25* expression in the skin leads to disruption of the epithelium and enhances HSV-1 and vaccinia virus replication [38]. MVC_eGFP cells are known to produce acetylcholine, which can activate sustentacular cells through M3 muscarinic acetylcholine receptors [63]. Sustentacular cells may in particular play a role in maintaining extracellular ionic gradients, extracellular glucose, secreting mucus, metabolizing noxious chemicals, and regulating cell turnover [25, 89]. In addition to *Il-25*, the expression of enzymes for eicosanoid biosynthesis (*Alox5*, *Ptgs1* and *Ptgs2*) suggests that MVC_eGFP are likely to recruit group 2 innate lymphoid cells, similar to tuft cells in the small intestine [55]. Finally, the innate immune response involves recruitment of macrophages that are known to play a protective role in the olfactory epithelium [6]. MVC_eGFP express the G-protein coupled receptor GPR126/ADGRG6, which is required for macrophage

recruitment and Schwann cells regeneration after peripheral nerve injury [58]. This raises the question whether MVC_eGFP could play a protective role, promoting OSN survival and increasing neurogenesis, through macrophage recruitment. In addition, activation of MVCs by irritants, bacteria and viruses could result in activation of cytokine-induced inflammation and macrophage recruitment by long-term horizontal basal cells, that activate type 1 immune responses within the olfactory epithelium [11]. All cytokines and interferons produced in the microenvironment of a MVC_eGFP can then contribute to the activation of immune responses in neighboring MVC_eGFP, since we found the expression of various cytokine receptors (*IL6ra*, *Il1rap*, *ILAra*, *IL17re*, *IL17 rb*, *TNFRSF13B*) and interferons responsive elements (*Ifitms*).

Our findings of expression of virally relevant transcripts in MVC_eGFP cells complement published studies on the role of MVC-related SCCs in viral infection. In the trachea, viral-associated formyl peptides activate SCCs to release acetylcholine and activate mucociliary clearance by ciliated cells [68]. This activation is mediated by the TRPM5 transduction pathway in the SCC and muscarinic acetylcholine receptors in the ciliated cell. In a similar manner in the olfactory epithelium MVCs respond to ATP, which is involved in activating mucociliary movement by releasing acetylcholine and activating adjacent sustentacular cells through a

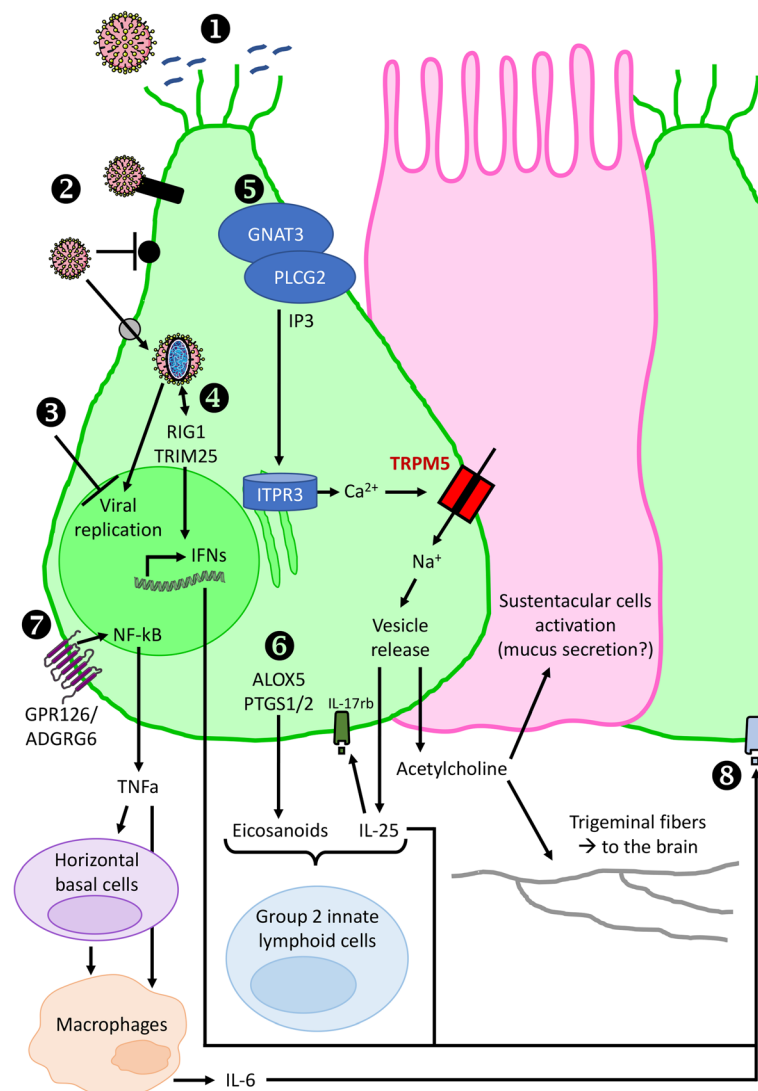


Fig. 6 Model depicting the role for microvillous cells involvement in the olfactory epithelium innate immune response to viral infection. 1) Secreted or cell surface glycoproteins constitute a first barrier preventing virus entry. 2) When reaching MVC_eGFP, viruses can encounter three types of membrane proteins: adhesion molecules that trigger intracellular signaling upon viral recognition (black rectangle), transmembrane proteins that block virus entry (black circle), viral receptors allowing virus entry (grey circle). 3) MVC_eGFP express numerous transcriptional factors involved in the inhibition of viral replication. 4) Cytosolic viral RNA sensing induces the production of type I interferons. 5) A possible signaling pathway leading to intracellular calcium increase, TRPM5 activation and Na⁺-mediated vesicle release. Acetylcholine can activate neighboring sustentacular cells and underlying trigeminal fibers. 6) Eicosanoids synthesis, along with IL-25 production, can recruit and activate group 2 innate lymphoid cells, which are key controllers of type 2 inflammation. 7) GPR126 activation results in NFκB activation and TNFα production. TNFα can directly activate macrophages. TNFα also induces a change in the function of horizontal basal cells, switching their phenotype from neuroregeneration to immune defense. 8) Interferons and cytokines can in turn activate antiviral immune response in neighboring MVC_eGFP

muscarinic receptor [25]. Therefore, viral infection could result in activation of MVCs resulting in activation of mucociliary clearance by adjacent sustentacular cells.

Pou2f3 also called *Skn1a*, encodes for a key regulator for the generation of TRPM5-expressing cells in various epithelial tissues [93]. *Pou2f3* transcript was increased in MVC_eGFP cells compared to OSN_eGFP⁻. *Skn1a/Pou2f3*-deficient mice lack intestinal tuft cells and have defective mucosal type 2 responses to helminth infection

in the intestine [29]. MVCs express markers of tuft cells (*Pou2f3*, *Trpm5* and others) indicating that MVCs share inflammatory and innate immune functions with tuft cells in the gut and SCCs and brush cells in the airways [84]. In addition, in the anterior olfactory epithelium, where there is a higher density of MVCs, mice exposed to mild odorous irritants exhibited a time-dependent increase in apoptosis and a loss of mature OSNs without a significant increase in proliferation or neurogenesis [43].

Future experiments are necessary to determine whether activation of MVCs by viruses could lead to loss of mature OSNs contributing to smell loss after viral infection. Interestingly, in the mouse distal lung, where there is no expression of SCCs, there was de novo generation of SCCs after infection with A/H1N1/PR/8 influenza virus [73] raising the question whether virus exposure could alter MVC number in the olfactory epithelium. Finally, in teleost fish rhabdoviruses induce apoptosis in a unique type of crypt OSN via the interaction of the OSN TrkA receptor with the viral glycoprotein and activates proinflammatory responses in the olfactory organ [77].

Viral infection of the central nervous system through the olfactory epithelium

The olfactory epithelium provides direct viral access to the brain through the olfactory nerve. Whether this olfactory path constitutes route of entry for viruses to the brain is a matter of intense discussion, especially because some viruses are postulated to be involved in encephalopathy and neurodegenerative disorders [10, 18, 20, 33]. Our finding that MVC_eGFP cells express virally-related genes at higher levels than OSN_eGFP⁻ cells suggests that these cells may be involved in or prevention of viral entry into the brain (and these two alternatives are not exclusive since they may be different for different viruses). On the one hand, we identified transcripts encoding for viral receptors in MVC_eGFP, suggesting that viruses can enter these cells. It is not known whether viruses can spread in neighboring cells, but if viral particles were to enter the OSNs they could reach the olfactory bulb through anterograde transport along the olfactory nerve and from the olfactory bulb, viruses can spread throughout the brain along the olfactory bulb-hippocampus route. On the other hand, we found enrichment for transcripts encoding for proteins involved in limiting viral infection and promoting immune and anti-inflammatory responses in MVC_eGFP cells. In this case, viral spread to the brain would be prevented. Finally, the olfactory epithelium is innervated by the trigeminal nerve, and substance P immunostaining is closely associated with subsets of MVCs [48]. This raises the question whether an interaction between MVCs and trigeminal nerve fibers could participate in local inflammation as found for SCCs [75], and could modulate the entry of virus to the brain stem through the trigeminal nerve. Future experiments are necessary to study the potential role of MVC_eGFP cells in viral infection of the olfactory epithelium and the brain.

Are GFP-expressing OSNs in the TRPM5-GFP mouse a distinct set of OSNs?

Expression of TRPM5 in a subset of OSNs has been controversial. The original proposal of expression of

TRPM5 in OSNs was motivated by expression of eGFP in adult TRPM5-eGFP transgenic mice and immunolabeling of the ciliary layer of the epithelium with an antibody (raised against the TRPM5 peptide RKEAQHKR QHLERDLDPDLDQK) that was validated by lack of expression in TRPM5 knockout mice [49]. However, staining in the ciliary layer with this antibody has not been replicated and our group and others subsequently showed knockout-validated TRPM5 staining of microvillous cells, and no labeling of the ciliary layer in the adult with antibodies raised against different TRPM5 protein peptides [28, 31, 48, 71]. Interestingly, Pyrski and co-workers found TRPM5 immunolabeling in OSNs in the embryo, but not in the adult [71]. Furthermore, in the adult mouse *in situ* hybridization has reported mRNA staining for TRPM5 in MVCs, and not in OSNs [71, 92], and full length TRPM5 mRNA was not found in OSNs in the adult [71].

Here we corroborate expression of eGFP in OSNs in TRPM5-eGFP transgenic mice. In addition, using HCR v3.0 we find strong expression of mRNA in MVCs, but we do not find evidence for expression of TRPM5 mRNA in OSNs (Fig. 5). However, transcriptional analysis indicates that the OSN_eGFP⁺ cell population differs in mRNA expression from the other two populations (Fig. 4). However, we have not verified expression of these transcripts or protein products with orthogonal methods. Thus, we have not validated that OSN_eGFP⁺ are a separate population of cells, and future studies will be necessary to address this issue.

Would microvillous cells play a role in COVID-19?

Recently, due to the current COVID-19 pandemic, researchers have focused their attention on investigating SARS-CoV-2 mechanism of entry into cells. SARS-CoV-2 targets mainly cells of the respiratory pathway where viral entry is mediated by ACE2 and TMPRSS2 [35]. Because numerous patients reported loss of smell [30, 66, 94, 95], researchers wondered about the mechanism for SARS-CoV-2 infection of the olfactory epithelium. In our study, we found the *Tmprss2* transcript was significantly increased in MVC_eGFP cells compared to OSN_eGFP⁻ (Fig. 3). We did not find *Ace2* enrichment in these cells, but this may be due to inefficiency in finding with RNAseq low abundance transcripts like *Ace2* [102]. Transcriptional profiling of single cells in the olfactory epithelium from other laboratories found expression of transcripts for both *Tmprss2* and *Ace2* in sustentacular cells and stem cells, and at lower levels in MVCs [7, 24]. Viral infection of sustentacular cells may explain loss of smell because these cells play a key role in supporting olfactory function by providing glucose for the energy necessary for olfactory transduction in the OSN cilia [89]. Importantly, type I interferons, and to a lesser

extent type II interferons induced by response of the host to SARS-CoV-2, and infection by other viruses inducing the interferon pathway increases *Ace2* expression in the nasal epithelium [102]. MVCs may play a role in SARS-CoV-2 infection of the olfactory epithelium because these cells may participate in activating inflammation of the epithelium that elicits type 1 immune response [11].

Conclusion

Here we find that microvillous cells of the olfactory epithelium express transcripts involved in immunity, inflammation and viral infection. These expression patterns suggest that, like tuft cells in the gut and SCCs and brush cells in the airways, the microvillous cells in the olfactory epithelium are involved in the innate immune response to viral infection. Our study provides new insights into a potential role for TRPM5-expressing cells in viral infection of the main olfactory epithelium.

Methods

Overview of the method for transcriptional profiling of low abundance cell populations

For transcriptional profiling of TRPM5-bearing MVC_eGFP cells and OSN_eGFP+ cells that constitute a small fraction of the cells in the epithelium, we used FACS to separate the cell populations targeted for RNAseq [3]. In our experiments, we isolated the cells from mice that expressed fluorescent marker proteins appropriate for cell sorting. OSNs were expressing mCherry under the control of OMP promoter. eGFP was expressed in MVCs and a subset of OSNs (OSN_eGFP+ cells) under control of the TRPM5 promoter.

Generation of OMP-H2B::cherry mice

A PacI cassette containing PacI-H2B::mCherry-pA PGK-puro-pA-PacI was inserted into an OMP gene-targeting vector (pPM9) [59], which replaces the OMP coding sequence with the PacI cassette and expresses a H2B::mCherry fusion protein. Animals are maintained in a mixed 129/B6 background.

Animals

Mice with TRPM5-driven eGFP expression [14] were crossed with OMP-H2B::Cherry mice. The TRPM5-eGFP mice and TRPM5 knockout mice [16] were obtained with written informed consent from Dr. Robert Margolskee. Lines were maintained separately as homozygous and backcrossed regularly. Experiments were performed on mice from the F1 generation cross of TRPM5-eGFP and OMP-H2B::Cherry mice (OMP-H2B::mCherry/TRPM5-eGFP). PCR was used to verify genotype of experimental mice for eGFP and mCherry expression. Both male and female mice were used for

experiments with ages ranging from 3 to 8 months. Estrous and cage mate information was collected for all female mice in conjunction with experimental use. Mice were housed in passive air exchange caging under a 12:12 light/dark cycle and were given food and water ad libitum. Mice were housed in the National Institutes of Health approved Center for Comparative Medicine at the University of Colorado Anschutz Medical Campus. All procedures were performed in compliance with University of Colorado Anschutz Medical Campus Institutional Animal Care and Use Committee (IACUC) that reviews the ethics of animal use. The total number of mice used in this study was 28 females and 50 males.

In our vivarium we have ventilated cages (HV cages) where air is mechanically exchanged with fresh air once every minute and static cages (LV cages) where air is exchanged passively through a filter in the cover. When we moved the OMP-H2B::mCherry/TRPM5-eGFP to HV cages we noticed a decrease in the number of OSN_eGFP+ cells sorted per mouse (Figure 1-figure supplement 1a, b and c), suggesting that changes in ventilation conditions affect TRPM5 promoter-driven expression of eGFP. Following this observation, mice were moved back to LV cages. We proceeded to study the dependence of the number of OSN_eGFP+ cells sorted on the number of days in LV vs. HV cages. The number of OSN_eGFP+ cells is positively correlated with the number of days the animal spends in LV cages (Figure 1 – figure supplement 1d) and negatively correlated to the number of days the animals spend in the HV cages (Figure 1 – figure supplement 1e). Generalized linear model (GLM) analysis found significant differences for the number of OSN_eGFP+ cells sorted as a function of the number of days in LV cages ($p < 0.05$, 26 observations, 24 d.f., F-statistic = 5.64, p -value for GLM < 0.05) and the number of days in HV cages ($p < 0.05$, 26 observations, 24 d.f., F-statistic = 5.99, p -value for GLM < 0.05). For RNAseq experiments one FACS sort was done using cells from mice born and maintained in HV housing, and the OSN_eGFP+ yield was low. Subsequently, we performed all FACS with cells isolated from the olfactory epithelium of mice raised in LV cages.

Tissue dissociation of the olfactory epithelium

Following euthanasia via CO₂ inhalation, the olfactory epithelium was immediately removed from the nasal cavity and epithelial tissue was separated from the bone in the turbinates. Care was taken not to include respiratory epithelium. The epithelium was dissociated enzymatically with Dispase II (2 mg/ml) diluted in Ringer's solution (145 mM NaCl, 5 mM KCL, 20 mM HEPES, 1 mM MgCl₂, 1 mM CaCl₂, 1 mM Ny-Pyruvate, 5 mM Glucose) (~ 25 min at 37 °C) followed by an incubation in a papain plus Ca/Mg++ free Ringer's solution (Ca/

Mg⁺⁺ free Ringer's: 145 mM NaCl, 5 mM KCL, 20 mM HEPES, 1 mM Ny-Pyruvate, 1 mM EDTA, L-cysteine: 1 mg L-cysteine /1.5 mL Ca/Mg⁺⁺ free Ringer's, Papain:1-3ul/1 mL Ca/Mg⁺⁺ free Ringer's), for ~40–45 min at 37 °C. Following incubation, DNase I (Promega) at 0.05 U/ μ l and RNase free 10x Reaction buffer (1:20) were added to solution and the tissue was gently triturated using a ~1 mm opening pipette. Isolated OSNs were collected from supernatants via centrifugation and resuspended in cell sorting medium of 1x PBS (diluted from commercial 10x PBS, pH 7.4) and BrainPhys Neuronal Medium (Stemcell Technologies). Initially, isolated cells were examined with a confocal microscope to confirm efficacy of dissociation methods, and examine cell types and fluorescence. For RNAseq, cells were strained through a 40 μ m cell strainer and kept on ice until sorted via flow cytometry.

Flow cytometry

Fluorescence activated cell sorting was performed in the University of Colorado Cancer Center Flow Cytometry Core on a Beckman Coulter MoFlo Astrios EQ using MoFlo Astrios Summit Software (6.3.1.16945). eGFP signal was detected using a 488 nm laser and a bandpass 526/52 nm collection filter. mCherry signal was detected using a 561 nm laser and a bandpass 614/20 nm collection filter. The 488 nm laser was also used to detect light scatter. The threshold was set at 3%. Gating was set to exclude doublets and optimized as cell populations emerged based on fluorescent markers. Flow cytometry calibration beads for AcGFP1/eGFP and mCherry (Takara, 632,594, 632,595) were used as fluorescence intensity controls. Olfactory epithelium cell suspensions from wild type and OMP-H2B::Cherry mice or TRPM5-eGFP mice were sorted as controls for auto fluorescence for eGFP and mCherry populations respectively. Cells were sorted into RNAprotect Tissue Reagent (Qiagen).

RNA-extraction

Total RNA was extracted from sorted, pooled cells from each cell population using the RNeasy Plus Micro Kit (Qiagen) according to the manufacturers recommended protocol.

RT-qPCR

Quantitative reverse transcription polymerase chain reaction (RT-qPCR) was used to assess and confirm identities of cell types from each of the sorted cell populations. Following total RNA extraction, RT-qPCR was performed in the PCR core at University of Colorado Anschutz Medical Campus for the following markers: OMP, TRPM5, eGFP and ChAT. Primers and probes used for eGFP, TRPM5 and OMP were described in [65]. Predesigned primers and probes for ChAT were

purchased from Life Technologies. The mRNA for these targets was measured by RT-qPCR using ABI QuantStudio 7 flex Sequence detector. One microgram total RNA was used to synthesize cDNA using the High Capacity c-DNA Reverse Transcription kit (ABI-P/N 4368814). cDNA was diluted 1: 2 before PCR amplification.

The TaqMan probes were 5' labeled with 6-carboxyfluorescein (FAM). Real time PCR reactions were carried out in MicroAmp optical tubes (PE ABI) in a 25 μ l mix containing 8% glycerol, 1X TaqMan buffer A (500 mM KCl, 100 mM Tris-HCl, 0.1 M EDTA, 600 nM passive reference dye ROX, pH 8.3 at room temperature), 300 μ M each of dATP, dGTP, dCTP and 600 μ M dUTP, 5.5 mM MgCl₂, 1X primer-probe mix, 1.25 U AmpliTaq Gold DNA and 5 μ l template cDNA. Thermal cycling conditions were as follows: Initiation was performed at 50 °C for 2 min followed by activation of TaqGold at 95 °C for 10 min. Subsequently 40 cycles of amplification were performed at 95 °C for 15 s and 60 °C for 1 min. Experiments were performed with duplicates for each data point. Each PCR run included the standard curve (10 fold serially diluted pooled cDNA from control and experimental samples), test samples, no-template and NORT controls. The standard curve was then used to calculate the relative amounts of targets in test samples. Quantities of targets in test samples were normalized to the corresponding 18 s rRNA (PE ABI, P/N 4308310).

RNA sequencing and pre-processing

RNA quality control, library preparation, and sequencing were performed at the University of Colorado Genomics and Microarray core. Extracted RNA was used as the input for the Nugen Universal Plus mRNA-seq kit (Redwood City, CA) to build stranded sequencing libraries. Indexed libraries were sequenced using an Illumina NovaSEQ6000. Library preparation and sequencing was performed in two batches, separated by gender. Eleven female samples were sequenced with an average depth of 37.3 million +/- SD of 6.5 million read pairs, and 25 male samples were sequenced with an average depth of 34.8 million +/- SD of 3.5 million read pairs. Metadata for the samples submitted are shown in Figure 2 - figure supplement 3. Raw BCL files were demultiplexed and converted to FASTQ format. Trimming, filtering, and adapter contamination removal was performed using BBDuk [9].

Sample size estimation was performed using R package 'RNASeqPower' [83]. A priori estimates were not performed for this study. Not all samples obtained from each mouse were of sufficient quality to proceed with RNA-sequencing and analysis. Samples for RNA-seq size were chosen based on the quality of cell sorting (sorts with groups with fewer than 2000 cells were excluded),

and overall RNA quality (the RIN score cutoff was 8). No samples were excluded for downstream RNA-seq processing. Randomization was not performed/applicable - each cell phenotype was collected from each animal. Blinding was not performed/applicable- data were processed with a standardized processing pipeline and no parameters were changed between comparisons.

Post-hoc analysis reveals that based on the gene variance coefficients of the data and the read coverage, we are powered to detect a linear fold change of 2 with a power of 0.8 using a minimum of 5 samples ($\alpha = 0.05$).

RNA sequencing analysis

Transcript abundance was quantified from trimmed and filtered FASTQ files using Salmon v1.2.1 [67] and a customized Ensembl GRCm38 (release 99) transcriptome [98]. A customized version of the transcriptome was prepared by appending FASTA sequences of eGFP and mCherry to the GRCm38 FASTA file. The corresponding gene transfer format (GTF) file was modified accordingly to incorporate the new transcripts. Transcript abundance was summarized at the gene level using the TxImport [82] package in R. Differential gene expression was quantified using DESeq2 [51] with default parameters after removing genes with an average count of < 5 reads in each group. Significance was determined by FDR-adjusted p -value < 0.05. TopGO was used for gene ontology analysis [1]. The input to TopGO was a list of significant DEGs and a list of all detected genes in the dataset. Enrichment was calculated by dividing the number of detected genes by the number of expected genes within each ontology of the TopGO output. To make the bar graphs in Figs. 4 and 5, enrichment scores of downregulated GO terms were multiplied by -1 for visualization. Heatmap visualization was performed using *pHeatmap* in R [39].

RNA-sequence data comparison with Ualiyeva et al [86]

Raw counts for this study and for Ualiyeva et al. (GEO GSE139014) [86] were converted to $\log_{10}(\text{reads per million (RPM)} + 1)$. These RPM values were used to generate heatmaps to show the expression values of specific transcripts. No quantitative assessment was performed between the two studies.

Tissue preparation for fluorescence microscopy and in situ

For euthanasia, mice were anesthetized with ketamine/xylazine (20–100 $\mu\text{g/g}$ of body weight), perfused transcardially with 0.1 M phosphate buffer (PBS) followed by a PBS-buffered fixative (EMS 32% Paraformaldehyde aqueous solution diluted to 4% with 1x PBS). The nose was harvested and postfixed for 12 h before being

transferred for cryoprotection into PBS with 20% sucrose overnight. The olfactory epithelium was cryosectioned coronally into 16 μm -thick sections mounted on Superfrost Plus slides (VWR, West Chester, PA) coated with poly-D-lysine.

In situ followed by immunohistochemistry (IHC)

In situ hybridization was performed with the hybridization chain reaction method [13] using HCR v3.0 Probe Sets, Amplifiers, and Buffers from Molecular Instruments, Inc. Frozen slides were allowed to thaw and dry, baked at 60 °C for 1 h, then immersed in 70% ethanol overnight at 4 °C, and allowed to dry again completely. Slides were inverted and placed on a Plexiglas platform inside a humidified chamber; subsequent steps were performed using this setup. Slides were incubated in 10 $\mu\text{g}/\mu\text{l}$ proteinase K for 15 min at 37 °C, then pre-hybridized with HCR hybridization buffer (30% formamide buffer from Molecular Instruments) for 30 min at 37 °C. *Trpm5-B3* probes and *OMP-B2* probes (0.8 pmol of each probe in 100 μl HCR hybridization buffer per slide) were added, and slides were hybridized overnight at 37 °C. Slides were briefly incubated in undiluted HCR Wash Buffer (30% formamide buffer from Molecular Instruments) for 20 min at 37 °C. Excess probes were removed by incubating slides for 20 min each at 37 °C in solutions of 75% HCR Wash Buffer / 25% SSCT (5X SSC, 0.1% Tween, diluted in RNase free water), 50% Buffer / 50% SSCT, 25% Buffer / 75% SSCT, and 100% SSCT. Slides were incubated in 100% SSCT at room temperature for 20 min, then in Amplification Buffer (Molecular Instruments) at room temperature for 1 h. B3 hairpins labeled with Alexa Fluor 647 and B2 hairpins labeled with Alexa Fluor 546 were prepared (12 pmol of each hairpin were heat shocked, then cooled for 30 min, and added to 200 μl of Amplification Buffer) added to slides, and incubated overnight at room temperature. Excess hairpins were removed with four washes (20 min) in SSCT at room temperature. Slides were then processed with IHC protocol to stain for GFP. At room temperature, tissue was permeabilized with Triton X-100 0.1% in PBS for 30 min, washed three times with PBS, blocked with Donkey serum 5% and Tween 20 0.3% in PBS for 1 h, incubated with Chicken anti-GFP primary antibody (1:500 in blocking solution, AB_2307313 Aves labs) overnight, washed three times with PBS and incubated with Donkey anti-Chicken secondary antibody conjugated with alexa fluor 488 (1:500 in blocking solution, 703–545-155 Jackson ImmunoResearch laboratories). After three final washes with PBS, slides were mounted using Fluoromount-G™ mounting medium with DAPI (Thermo Fisher Scientific).

Confocal fluorescence microscopy

Microscopy was performed with confocal microscopes (Leica SP8, Nikon A1R or 3i Marianas).

Three-dimensional tissue imaging

For three-dimensional imaging, a high numerical aperture (NA) oblique plane microscope was used [21, 74]. Briefly, this variant on a light sheet microscope only uses one objective to interface with the sample. The sample is illuminated from the epi-direction using an obliquely launched light sheet. Emitted fluorescence is detected through the same primary objective used for illumination. A secondary and tertiary objective optically resample the emitted fluorescence to image the fluorescence resulting from the obliquely launched light sheet onto a detector [21, 74]. For the primary, secondary, and tertiary objectives we used a high-NA silicone immersion objective (Nikon $\times 100$ NA 1.35, 0.28–0.31 mm working distance), a high-NA air immersion objective (Nikon $\times 40$ NA 0.95, 0.25–0.16 mm working distance), and a bespoke glass-tipped objective (AMS-AGY v1.0, NA 1.0, 0 mm working distance), respectively. Images were acquired by a high-speed scientific CMOS camera (Photometrics Prime BSI) using custom Python software ([74], <https://github.com/qi2lab/opm>).

The obliquely launched light sheet was set to 30 degrees above the coverslip. The sample was translated in one lateral dimension (x) at a constant speed by a scan optimized stage. The scan speed was set so that images with a 5-millisecond exposure time were acquired at 200 nm spacing over a distance of 5.5 mm. This constant speed scan was performed for the same volume, cycling through three excitation wavelengths (405, 488, 635 nm) and three sample height positions (z), with 20% overlap. Once the cycle of wavelengths and height positions completed, the sample was then laterally displaced (y), again with a 20% overlap, and the scan was repeated over a 5.5 mm \times 5.5 mm \times .035 mm (x,y,z) imaging volume. Raw data was orthogonally deskewed, stitched, and fused using custom Python code and BigStitcher [36]. After export, each inset image was deconvolved using Microvolution and measured point spread functions.

Statistical analysis

Statistical analysis was performed in Matlab (Mathworks, USA). Statistical significance was estimated using a generalized linear model (GLM), with post-hoc tests for all data pairs corrected for multiple comparisons using false discovery rate [15]. The post hoc comparisons between pairs of data were performed either with a t-test, or a ranksum test, depending on the result of an Anderson-Darling test of normality. 95% CIs shown in the figures as vertical black lines or shading bounding the lines were estimated by bootstrap analysis of the mean by sampling with replacement 1000 times using the bootci function in MATLAB.

Abbreviations

COVID-19: Coronavirus disease 2019; DPI: Days post infection; eGFP: Enhanced green fluorescent protein; FACS: Fluorescence-activated cell sorting; FDR: False discovery rate; GLM: Generalized linear model; GO: Gene ontology; MVCs: Microvillous cells; OMP: Olfactory marker protein; OSNs: Olfactory sensory neurons; PSF: Point spread function; SARS-CoV-2: Severe acute respiratory syndrome coronavirus clade 2; SSC: Saline-sodium citrate; SSCT: SSC with tween; TRPM5: Transient receptor potential cation channel subfamily M member 5

Supplementary Information

The online version contains supplementary material available at <https://doi.org/10.1186/s12864-021-07528-y>.

Additional file 1.

Additional file 2.

Acknowledgements

We would like to acknowledge the support of Nicole Arevalo for laboratory support, Jerome Artus and Anna-Katerina Hadjantonakis for the construction of the targeting vector and production of OMP-H2B::Cherry mice, Emily Liman for providing TRPM5 and TRPC2 antibody and Catherine Dulac for providing tissue from TRPC2 knockouts.

Authors' contributions

D.R., B.D.B., M.A.N. and V.R.R. conceptualized the project. B.D.B. performed FACS, qPCR and RNAseq experiments. E.D.L. performed genomic analysis. P.F. generated the OMP-H2B::Cherry mice. M.A.N., A.N.B. and C.S.N. designed experiments. A.G.P., C.S.N. and J.H.Jr. performed experiments. D.S. designed and analyzed in situ experiments. L.M. performed in situ experiments and literature search and wrote the section on viral infection in the discussion. All authors contributed to writing and editing the manuscript. The author(s) read and approved the final manuscript.

Funding

This work was supported by NIDCD DC014253 and NIA DC014253-04S1 (DR), by the RNA Bioscience Initiative of the University of Colorado Anschutz Medical Campus (DS and DR) and by NIDCD R21DC018864 (EDL). A Starr Stem Cell Grant (JA, AKH and PF) supported the production and characterization of the OMP-H2B::mCherry mouse strain. The funding bodies had no role in the experimental design or collection, analysis and interpretation of data or in writing the manuscript.

Availability of data and materials

All data sequencing data are available in NCBI SRA <https://www.ncbi.nlm.nih.gov/sra/PRJNA632936>. The code used for bioinformatics analysis is found in https://github.com/eric-d-larson/OE_TRPM5

Declarations

Ethics approval

Mouse experiments were carried out under guidelines of the National Institutes of Health in compliance with University of Colorado Anschutz Medical Campus Institutional Animal Care and Use Committee (IACUC).

Consent for publication

Not applicable.

Competing interests

The authors declare no competing interests.

Author details

¹Neuroscience Graduate Program, University of Colorado Anschutz Medical Campus, Aurora, CO 80045, USA. ²Department of Cell and Developmental Biology, University of Colorado Anschutz Medical Campus, Aurora, CO 80045, USA. ³Department of Otolaryngology, University of Colorado Anschutz Medical Campus, Aurora, CO 80045, USA. ⁴The Graduate Center Biochemistry, Biology and CUNY-Neuroscience-Collaborative Programs and Biological Sciences Department, Hunter College, City University of New York, New York,

NY 10065, USA. ⁵Department of Neurology, University of Colorado Anschutz Medical Campus, Aurora, CO 80045, USA. ⁶Department of Pharmacology, University of Colorado Anschutz Medical Campus and Center for Biological Physics and Department of Physics, Arizona State University, Tempe, USA.

Received: 8 June 2020 Accepted: 12 March 2021

Published online: 30 March 2021

References

- Alexa A, Rahnenfuhrer J. topGO: Enrichment Analysis for Gene Ontology (R Package); 2020.
- Allaire A, Picard-Jean F, Bisaillon M. Immunofluorescence to Monitor the Cellular Uptake of Human Lactoferrin and its Associated Antiviral Activity Against the Hepatitis C Virus. *J Vis Exp*. 2015;104:53053.
- Amamoto R, Garcia MD, West ER, Choi J, Lapan SW, Lane EA, et al. Probe-Seq enables transcriptional profiling of specific cell types from heterogeneous tissue by RNA-based isolation. *Elife*. 2019;8:e51452. <https://doi.org/10.7554/eLife.51452>.
- Bankova LG, Dwyer DF, Yoshimoto E, Ualiyeva S, McGinty JW, Raff H, et al. The cysteinyl leukotriene 3 receptor regulates expansion of IL-25-producing airway brush cells leading to type 2 inflammation. *Sci Immunol*. 2018;3:eat9453.
- Bastianelli E, Polans AS, Hidaka H, Pochet R. Differential distribution of six calcium-binding proteins in the rat olfactory epithelium during postnatal development and adulthood. *J Comp Neurol*. 1995;354(3):395–409. <https://doi.org/10.1002/cne.903540308>.
- Borders AS, Getchell ML, Etscheidt JT, van Rooijen N, Cohen DA, Getchell TV. Macrophage depletion in the murine olfactory epithelium leads to increased neuronal death and decreased neurogenesis. *J Comp Neurol*. 2007;501(2):206–18. <https://doi.org/10.1002/cne.21252>.
- Brann DH, Tsukahara T, Weinreb C, Lipovsek M, Van den Berge K, Gong B, et al. Non-neuronal expression of SARS-CoV-2 entry genes in the olfactory system suggests mechanisms underlying COVID-19-associated anosmia. *Sci Adv*. 2020;6:eabc5801.
- Brass AL, Huang IC, Benita Y, John SP, Krishnan MN, Feeley EM, et al. The IFITM proteins mediate cellular resistance to influenza A H1N1 virus, West Nile virus, and dengue virus. *Cell*. 2009;139(7):1243–54. <https://doi.org/10.1016/j.cell.2009.12.017>.
- BBMap – Bushnell B. – <http://www.sourceforge.net/projects/bbmap/>.
- Cairns DM, Rouleau N, Parker RN, Walsh KG, Gehrke L, Kaplan DL. A 3D human brain-like tissue model of herpes-induced Alzheimer's disease. *Sci Adv*. 2020;6:eaay8828.
- Chen M, Reed RR, Lane AP. Chronic inflammation directs an olfactory stem cell functional switch from Neuroregeneration to immune defense. *Cell Stem Cell*. 2019;25(501–513):e505.
- Cheshenko N, Pierce C, Herold BC. Herpes simplex viruses activate phospholipid scramblase to redistribute phosphatidylserines and Akt to the outer leaflet of the plasma membrane and promote viral entry. *PLoS Pathog*. 2018;14(1):e1006766. <https://doi.org/10.1371/journal.ppat.1006766>.
- Choi HM, Schwarzkopf M, Fornace ME, Acharya A, Artavanis G, Stegmaier J, et al. Third-generation in situ hybridization chain reaction: multiplexed, quantitative, sensitive, versatile, robust. *Development*. 2018;145:dev165753.
- Clapp TR, Medler KF, Damak S, Margolskee RF, Kinnamon SC. Mouse taste cells with G protein-coupled taste receptors lack voltage-gated calcium channels and SNAP-25. *BMC Biol*. 2006;4(1):7. <https://doi.org/10.1186/1741-7007-4-7>.
- Curran-Everett D. Multiple comparisons: philosophies and illustrations. *Am J Phys Regul Integr Comp Phys*. 2000;279:R1–8.
- Damak S, Rong M, Yasumatsu K, Kokrashvili Z, Perez CA, et al. Trpm5 null mice respond to bitter, sweet, and umami compounds. *Chem Senses*. 2006;31(3):253–64. <https://doi.org/10.1093/chemse/bjj027>.
- Damak S, Rong M, Yasumatsu K, Kokrashvili Z, Varadarajan V, Zou S, et al. Detection of sweet and umami taste in the absence of taste receptor T1r3. *Science*. 2003;301(5634):850–3. <https://doi.org/10.1126/science.1087155>.
- Dando SJ, Mackay-Sim A, Norton R, Currie BJ, St John JA, Ekberg JAK, et al. Pathogens penetrating the central nervous system: infection pathways and the cellular and molecular mechanisms of invasion. *Clin Microbiol Rev*. 2014;27(4):691–726. <https://doi.org/10.1128/CMR.00118-13>.
- Dong C, Sun X, Guan Z, Zhang M, Duan M. Modulation of influenza A virus replication by microRNA-9 through targeting MCP1P1. *J Med Virol*. 2017;89(1):41–8. <https://doi.org/10.1002/jmv.24604>.
- Doty RL. The olfactory vector hypothesis of neurodegenerative disease: is it viable? *Ann Neurol*. 2008;63(1):7–15. <https://doi.org/10.1002/ana.21327>.
- Dunsby C. Optically sectioned imaging by oblique plane microscopy. *Opt Express*. 2008;16(25):20306–16. <https://doi.org/10.1364/OE.16.020306>.
- Farbman AI, Margolis FL. Olfactory marker protein during ontogeny: immunohistochemical localization. *Dev Biol*. 1980;74(1):205–15. [https://doi.org/10.1016/0012-1606\(80\)90062-7](https://doi.org/10.1016/0012-1606(80)90062-7).
- Fischl AM, Heron PM, Stromberg AJ, McClintock TS. Activity-dependent genes in mouse olfactory sensory neurons. *Chem Senses*. 2014;39(5):439–49. <https://doi.org/10.1093/chemse/bju015>.
- Fodoulian L, Tuberosa J, Rossier D, Landis BN, Carleton A, Rodriguez I. SARS-CoV-2 receptor and entry genes are expressed by sustentacular cells in the human olfactory neuroepithelium. *bioRxiv*. 2020:2020.2003.2031.013268.
- Fu Z, Ogura T, Luo W, Lin W. ATP and odor mixture activate TRPM5-expressing microvillous cells and potentially induce acetylcholine release to enhance supporting cell endocytosis in mouse Main olfactory epithelium. *Front Cell Neurosci*. 2018;12:71. <https://doi.org/10.3389/fncel.2018.00071>.
- Gack MU, Albrecht RA, Urano T, Inn KS, Huang IC, Carnero E, et al. Influenza A virus NS1 targets the ubiquitin ligase TRIM25 to evade recognition by the host viral RNA sensor RIG-I. *Cell Host Microbe*. 2009;5(5):439–49. <https://doi.org/10.1016/j.chom.2009.04.006>.
- Gack MU, Shin YC, Joo CH, Urano T, Liang C, Sun L, et al. TRIM25 RING-finger E3 ubiquitin ligase is essential for RIG-I-mediated antiviral activity. *Nature*. 2007;446(7138):916–20. <https://doi.org/10.1038/nature05732>.
- Genovese F, Tizzano M. Microvillous cells in the olfactory epithelium express elements of the solitary chemosensory cell transduction signaling cascade. *PLoS One*. 2018;13(9):e0202754. <https://doi.org/10.1371/journal.pone.0202754>.
- Gerbe F, Sidot E, Smyth DJ, Ohmoto M, Matsumoto I, Dardalhon V, et al. Intestinal epithelial tuft cells initiate type 2 mucosal immunity to helminth parasites. *Nature*. 2016;529(7585):226–30. <https://doi.org/10.1038/nature16527>.
- Giacomelli A, Pezzati L, Conti F, Bernacchia D, Siano M, Oreni L, et al. Self-reported olfactory and taste disorders in SARS-CoV-2 patients: a cross-sectional study. *Clin Infect Dis*. 2020;71(15):889–90. <https://doi.org/10.1093/cid/ciaa330>.
- Gilbert MA, Lin B, Peterson J, Jang W, Schwob JE. Neuregulin1 and ErbB expression in the uninjured and regenerating olfactory mucosa. *Gene Expr Patterns*. 2015;19(1-2):108–19. <https://doi.org/10.1016/j.gexp.2015.10.001>.
- Gong Q, Cheng M, Chen H, Liu X, Si Y, Yang Y, et al. Phospholipid scramblase 1 mediates hepatitis C virus entry into host cells. *FEBS Lett*. 2011;585(17):2647–52. <https://doi.org/10.1016/j.febslet.2011.07.019>.
- Harris SA, Harris EA. Molecular mechanisms for herpes simplex virus type 1 pathogenesis in Alzheimer's disease. *Front Aging Neurosci*. 2018;10:48. <https://doi.org/10.3389/fnagi.2018.00048>.
- Hegg CC, Jia C, Chick WS, Restrepo D, Hansen A. Microvillous cells expressing IP3 receptor type 3 in the olfactory epithelium of mice. *Eur J Neurosci*. 2010;32(10):1632–45. <https://doi.org/10.1111/j.1460-9568.2010.07449.x>.
- Hoffmann M, Kleine-Weber H, Schroeder S, Kruger N, Herrler T, Erichsen S, et al. SARS-CoV-2 cell entry depends on ACE2 and TMPRSS2 and is blocked by a clinically proven protease inhibitor. *Cell*. 2020;181:271–280 e278.
- Hörl D, Rojas Rusak F, Preusser F, Tillberg P, Randel N, Chhetri RK, et al. BigStitcher: reconstructing high-resolution image datasets of cleared and expanded samples. *Nat Methods*. 2019;16(9):870–4. <https://doi.org/10.1038/s41592-019-0501-0>.
- Juilfs DM, Fulle HJ, Zhao AZ, Houslay MD, Garbers DL, Beavo JA. A subset of olfactory neurons that selectively express cGMP-stimulated phosphodiesterase (PDE2) and guanylyl cyclase-D define a unique olfactory signal transduction pathway. *Proc Natl Acad Sci U S A*. 1997;94(7):3388–95. <https://doi.org/10.1073/pnas.94.7.3388>.
- Kim BE, Bin L, Ye YM, Ramamoorthy P, Leung DYM. IL-25 enhances HSV-1 replication by inhibiting filaggrin expression, and acts synergistically with Th2 cytokines to enhance HSV-1 replication. *J Invest Dermatol*. 2013;133(12):2678–85. <https://doi.org/10.1038/jid.2013.223>.
- Kolde, R. (2019). pheatmap: Pretty Heatmaps (cran.r-project.org).
- Kopp SJ, Banisadr G, Glajch K, Maurer UE, Grunewald K, Miller RJ, et al. Infection of neurons and encephalitis after intracranial inoculation of herpes simplex virus requires the entry receptor nectin-1. *Proc Natl Acad Sci U S A*. 2009;106(42):17916–20. <https://doi.org/10.1073/pnas.0908892106>.
- Lee WJ, Fu RM, Liang C, Sloan RD. IFITM proteins inhibit HIV-1 protein synthesis. *Sci Rep*. 2018;8(1):14551. <https://doi.org/10.1038/s41598-018-32785-5>.

42. Lemons K, Fu Z, Aoude I, Ogura T, Sun J, Chang J, et al. Lack of TRPM5-expressing microvillous cells in mouse Main olfactory epithelium leads to impaired odor-evoked responses and olfactory-guided behavior in a challenging chemical environment. *eNeuro*. 2017;4(3):ENEURO.0135-17.2017.
43. Lemons K, Fu Z, Ogura T, Lin W. TRPM5-expressing microvillous cells regulate region-specific cell proliferation and apoptosis during chemical exposure. *Neuroscience*. 2020;434:171–90. <https://doi.org/10.1016/j.neuroscience.2020.03.029>.
44. Li H, Handsaker B, Wysoker A, Fennell T, Ruan J, Homer N, et al. The sequence alignment/map format and SAMtools. *Bioinformatics*. 2009;25:2078–9.
45. Li M, Yang J, Zhao Y, Song Y, Yin S, Guo J, et al. MCP1 inhibits hepatitis B virus replication by destabilizing viral RNA and negatively regulates the virus-induced innate inflammatory responses. *Antivir Res*. 2020;174:104705. <https://doi.org/10.1016/j.antiviral.2020.104705>.
46. Liberles SD. Trace amine-associated receptors: ligands, neural circuits, and behaviors. *Curr Opin Neurobiol*. 2015;34:1–7. <https://doi.org/10.1016/j.conb.2015.01.001>.
47. Lin RJ, Chu JS, Chien HL, Tseng CH, Ko PC, Mei YY, et al. MCP1 suppresses hepatitis C virus replication and negatively regulates virus-induced proinflammatory cytokine responses. *J Immunol*. 2014;193(8):4159–68. <https://doi.org/10.4049/jimmunol.1400337>.
48. Lin W, Ezekwe EA Jr, Zhao Z, Liman ER, Restrepo D. TRPM5-expressing microvillous cells in the main olfactory epithelium. *BMC Neurosci*. 2008;9(1):114. <https://doi.org/10.1186/1471-2202-9-114>.
49. Lin W, Margolskee R, Donnet G, Hell SW, Restrepo D. Olfactory neurons expressing transient receptor potential channel M5 (TRPM5) are involved in sensing semiochemicals. *Proc Natl Acad Sci U S A*. 2007;104(7):2471–6. <https://doi.org/10.1073/pnas.0610201104>.
50. Lopez F, Delgado R, Lopez R, Bacigalupo J, Restrepo D. Transduction for pheromones in the Main olfactory epithelium is mediated by the Ca²⁺-Activated Channel TRPM5. *J Neurosci*. 2014;34(9):3268–78. <https://doi.org/10.1523/JNEUROSCI.4903-13.2014>.
51. Love MI, Huber W, Anders S. Moderated estimation of fold change and dispersion for RNA-seq data with DESeq2. *Genome Biol*. 2014;15(12):550. <https://doi.org/10.1186/s13059-014-0550-8>.
52. Luo W, Zhang J, Liang L, Wang G, Li Q, Zhu P, et al. Phospholipid scramblase 1 interacts with influenza A virus NP, impairing its nuclear import and thereby suppressing virus replication. *PLoS Pathog*. 2018;14(1):e1006851. <https://doi.org/10.1371/journal.ppat.1006851>.
53. Luo XC, Chen ZH, Xue JB, Zhao DX, Lu C, Li YH, et al. Infection by the parasitic helminth *Trichinella spiralis* activates a Tas2r-mediated signaling pathway in intestinal tuft cells. *Proc Natl Acad Sci U S A*. 2019;116(12):5564–9. <https://doi.org/10.1073/pnas.1812901116>.
54. Maina IW, Workman AD, Cohen NA. The role of bitter and sweet taste receptors in upper airway innate immunity: recent advances and future directions. *World J Otorhinolaryngol Head Neck Surg*. 2018;4(3):200–8. <https://doi.org/10.1016/j.wjorl.2018.07.003>.
55. McGinty JW, Ting H-A, Billipp TE, Nadsjombati MS, Khan DM, Barrett NA, et al. Tuft-cell-derived Leukotrienes drive rapid anti-helminth immunity in the small intestine but are dispensable for anti-protist immunity. *Immunity*. 2020;52:528–541.e527.
56. McLaughlin SK, McKinnon PJ, Margolskee RF. Gustducin is a taste-cell-specific G protein closely related to the transducins. *Nature*. 1992;357(6379):563–9. <https://doi.org/10.1038/357563a0>.
57. Meyerson NR, Zhou L, Guo YR, Zhao C, Tao YJ, Krug RM, et al. Nuclear TRIM25 specifically targets influenza virus Ribonucleoproteins to block the onset of RNA chain elongation. *Cell Host Microbe*. 2017;22:627–638.e627.
58. Mogha A, Harty BL, Carlin D, Joseph J, Sanchez NE, Suter U, et al. Gpr126/Adgrg6 has Schwann cell autonomous and nonautonomous functions in peripheral nerve injury and repair. *J Neurosci*. 2016;36(49):12351–67. <https://doi.org/10.1523/JNEUROSCI.3854-15.2016>.
59. Mombaerts P, Wang F, Dulac C, Chao SK, Nemes A, Mendelsohn M, et al. Visualizing an olfactory sensory map. *Cell*. 1996;87(4):675–86. [https://doi.org/10.1016/S0092-8674\(00\)81387-2](https://doi.org/10.1016/S0092-8674(00)81387-2).
60. Narayana SK, Helbig KJ, McCartney EM, Eyre NS, Bull RA, Eltahla A, et al. The interferon-induced Transmembrane proteins, IFITM1, IFITM2, and IFITM3 inhibit hepatitis C virus entry. *J Biol Chem*. 2015;290(43):25946–59. <https://doi.org/10.1074/jbc.M115.657346>.
61. Noyce RS, Richardson CD. Nectin 4 is the epithelial cell receptor for measles virus. *Trends Microbiol*. 2012;20(9):429–39. <https://doi.org/10.1016/j.tim.2012.05.006>.
62. O'Leary CE, Schneider C, Locksley RM. Tuft cells-systemically dispersed sensory epithelia integrating immune and neural circuitry. *Annu Rev Immunol*. 2019;37(1):47–72. <https://doi.org/10.1146/annurev-immunol-042718-041505>.
63. Ogura T, Szebenyi SA, Krosnowski K, Sathyanesan A, Jackson J, Lin W. Cholinergic microvillous cells in the mouse main olfactory epithelium and effect of acetylcholine on olfactory sensory neurons and supporting cells. *J Neurophysiol*. 2011;106(3):1274–87. <https://doi.org/10.1152/jn.00186.2011>.
64. Omura M, Mombaerts P. Trpc2-expressing sensory neurons in the Main olfactory epithelium of the mouse. *Cell Rep*. 2014;8(2):583–95. <https://doi.org/10.1016/j.celrep.2014.06.010>.
65. Oshimoto A, Wakabayashi Y, Garske A, Lopez R, Rolen S, Flowers M, et al. Potential role of transient receptor potential channel M5 in sensing putative pheromones in mouse olfactory sensory neurons. *PLoS One*. 2013;8(4):e61990. <https://doi.org/10.1371/journal.pone.0061990>.
66. Parma V, Ohla K, Veldhuizen MG, Niv MY, Kelly CE, Bakke AJ, et al. More than smell – COVID-19 is associated with severe impairment of smell, taste, and chemesthesis. *Chem Senses*. 2020;45(7):609–22. <https://doi.org/10.1093/chemse/bjaa041>.
67. Patro R, Duggal G, Love MI, Irizarry RA, Kingsford C. Salmon provides fast and bias-aware quantification of transcript expression. *Nat Methods*. 2017;14(4):417–9. <https://doi.org/10.1038/nmeth.4197>.
68. Perniss A, Liu S, Boonen B, Keshavarz M, Ruppert AL, et al. Chemosensory cell-derived acetylcholine drives tracheal mucociliary clearance in response to virulence-associated Formyl peptides. *Immunity*. 2020;52:683–699.e611.
69. Petermann P, Rahn E, Thier K, Hsu MJ, Rixon FJ, Kopp SJ, et al. Role of Nectin-1 and Herpesvirus entry mediator as cellular receptors for herpes simplex virus 1 on primary murine dermal fibroblasts. *J Virol*. 2015;89(18):9407–16. <https://doi.org/10.1128/JVI.01415-15>.
70. Pomaznoy M, Ha B, Peters B. GOnet: a tool for interactive gene ontology analysis. *BMC Bioinformatics*. 2018;19(1):470. <https://doi.org/10.1186/s12859-018-2533-3>.
71. Pyrski M, Eckstein E, Schmid A, Bufer B, Weiss J, Chubanov V, et al. Trpm5 expression in the olfactory epithelium. *Mol Cell Neurosci*. 2017;80:75–88. <https://doi.org/10.1016/j.mcn.2017.02.002>.
72. Pyrski M, Tusty M, Eckstein E, Oboti L, Rodriguez-Gil DJ, Greer CA, et al. P/Q type Calcium Channel Cav2.1 defines a unique subset of glomeruli in the mouse olfactory bulb. *Front Cell Neurosci*. 2018;12:295.
73. Rane CK, Jackson SR, Pastore CF, Zhao G, Weiner AI, Patel NN, et al. Development of solitary chemosensory cells in the distal lung after severe influenza injury. *Am J Phys Lung Cell Mol Phys*. 2019;316(6):L1141–9. <https://doi.org/10.1152/ajplung.00032.2019>.
74. Sapoznik E, Chang B-J, Huh J, Ju RJ, Azarova EV, Pohlkamp T, et al. A versatile oblique plane microscope for large-scale and high-resolution imaging of subcellular dynamics. *eLife*. 2020;9:e57681. <https://doi.org/10.7554/eLife.57681>.
75. Saunders CJ, Christensen M, Finger TE, Tizzano M. Cholinergic neurotransmission links solitary chemosensory cells to nasal inflammation. *Proc Natl Acad Sci U S A*. 2014;111(16):6075–80. <https://doi.org/10.1073/pnas.1402251111>.
76. Sayers S, Elliott G. Herpes simplex virus 1 enters human keratinocytes by a Nectin-1-dependent, rapid plasma membrane fusion pathway that functions at low temperature. *J Virol*. 2016;90(22):10379–89. <https://doi.org/10.1128/M.01582-16>.
77. Sepahi A, Kraus A, Casadei E, Johnston CA, Galindo-Villegas J, Kelly C, et al. Olfactory sensory neurons mediate ultrarapid antiviral immune responses in a TrkA-dependent manner. *Proc Natl Acad Sci*. 2019;116(25):12428–36. <https://doi.org/10.1073/pnas.1900083116>.
78. Shestakov A, Jenssen H, Nordstrom I, Eriksson K. Lactoferrin but not lactoferrin inhibit herpes simplex virus type 2 infection in mice. *Antivir Res*. 2012;93(3):340–5. <https://doi.org/10.1016/j.antiviral.2012.01.003>.
79. Shukla ND, Tiwari V, Valyi-Nagy T. Nectin-1-specific entry of herpes simplex virus 1 is sufficient for infection of the cornea and viral spread to the trigeminal ganglia. *Mol Vis*. 2012;18:2711–6.
80. Singh BK, Hornick AL, Krishnamurthy S, Locke AC, Mendoza CA, Mateo M, et al. The Nectin-4/Afadin protein complex and intercellular membrane pores contribute to rapid spread of measles virus in primary human airway epithelia. *J Virol*. 2015;89(14):7089–96. <https://doi.org/10.1128/JVI.00821-15>.
81. Singh BK, Li N, Mark AC, Mateo M, Cattaneo R, Sinn PL. Cell-to-cell contact and Nectin-4 govern spread of measles virus from primary human myeloid cells to primary human airway epithelial cells. *J Virol*. 2016;90(15):6808–17. <https://doi.org/10.1128/JVI.00266-16>.

82. Soneson C, Love MI, Robinson MD. Differential analyses for RNA-seq: transcript-level estimates improve gene-level inferences. *F1000Res*. 2015;4:1521.
83. Therneau T, Hart S, Kocher J. Calculating sample size estimates for RNA Seq studies. R package version 1.30.0; 2020.
84. Ting H-A, von Moltke J. The immune function of tuft cells at gut mucosal surfaces and beyond. *J Immunol*. 2019;202(5):1321–9. <https://doi.org/10.4049/jimmunol.1801069>.
85. Tizzano M, Gulbransen BD, Vandenbeuch A, Clapp TR, Herman JP, Sibhatu HM, et al. Nasal chemosensory cells use bitter taste signaling to detect irritants and bacterial signals. *Proc Natl Acad Sci U S A*. 2010;107(7):3210–5. <https://doi.org/10.1073/pnas.0911934107>.
86. Ualiyeva S, Hallen N, Kanaoka Y, Ledderose C, Matsumoto I, Junger W, et al. Airway brush cells generate cysteinyl leukotrienes through the ATP sensor P2Y2. *Sci Immunol*. 2020;5(43):eaax7224. <https://doi.org/10.1126/sciimmunol.aax7224>.
87. Valimaa H, Tenovuori J, Waris M, Hukkanen V. Human lactoferrin but not lysozyme neutralizes HSV-1 and inhibits HSV-1 replication and cell-to-cell spread. *Virology*. 2009;61(1):53. <https://doi.org/10.1016/j.virus.2008.11.013>.
88. van der Linden C, Jakob S, Gupta P, Dulac C, Santoro SW. Sex separation induces differences in the olfactory sensory receptor repertoires of male and female mice. *Nat Commun*. 2018;9(1):5081. <https://doi.org/10.1038/s41467-018-07120-1>.
89. Villar PS, Delgado R, Vergara C, Reyes JG, Bacigalupo J. Energy requirements of odor transduction in the chemosensory cilia of olfactory sensory neurons rely on oxidative phosphorylation and glycolytic processing of extracellular glucose. *J Neurosci*. 2017;37(23):5736–43. <https://doi.org/10.1523/JNEUROSCI.2640-16.2017>.
90. von Moltke J, Ji M, Liang HE, Locksley RM. Tuft-cell-derived IL-25 regulates an intestinal ILC2-epithelial response circuit. *Nature*. 2016;529(7585):221–5. <https://doi.org/10.1038/nature16161>.
91. Wilen CB, Lee S, Hsieh LL, Orchard RC, Desai C, Hykes BL, et al. Tropism for tuft cells determines immune promotion of norovirus pathogenesis. *Science*. 2018;360(6385):204–8. <https://doi.org/10.1126/science.aar3799>.
92. Yamaguchi T, Yamashita J, Ohmoto M, Aoude I, Ogura T, Luo W, et al. Skn-1a/Pou2f3 is required for the generation of Trpm5-expressing microvillous cells in the mouse main olfactory epithelium. *BMC Neurosci*. 2014;15(1):13. <https://doi.org/10.1186/1471-2202-15-13>.
93. Yamashita J, Ohmoto M, Yamaguchi T, Matsumoto I, Hirota J. Skn-1a/Pou2f3 functions as a master regulator to generate Trpm5-expressing chemosensory cells in mice. *PLoS One*. 2017;12(12):e0189340. <https://doi.org/10.1371/journal.pone.0189340>.
94. Yan CH, Faraji F, Prajapati DP, Boone CE, DeConde AS. Association of chemosensory dysfunction and Covid-19 in patients presenting with influenza-like symptoms. *Int Forum Allergy Rhinol*. 2020: 10.1002/alar.22579. <https://doi.org/10.1002/alar.22579>. [Epub ahead of print].
95. Yan CH, Faraji F, Prajapati DP, Ostrander BT, DeConde AS. Self-reported olfactory loss associates with outpatient clinical course in Covid-19. *Int Forum Allergy Rhinol*. 2020b.
96. Yang J, Zhu X, Liu J, Ding X, Han M, Hu W, et al. Inhibition of hepatitis B virus replication by phospholipid scramblase 1 in vitro and in vivo. *Antiviral Res*. 2012;94(1):9–17. <https://doi.org/10.1016/j.antiviral.2012.01.010>.
97. Yu J, Li M, Wilkins J, Ding S, Swartz TH, Esposito AM, et al. IFITM proteins restrict HIV-1 infection by antagonizing the envelope glycoprotein. *Cell Rep*. 2015;13(1):145–56. <https://doi.org/10.1016/j.celrep.2015.08.055>.
98. Zerbino DR, Achuthan P, Akanni W, Amode MR, Barrell D, Bhai J, et al. Ensembl 2018. *Nucleic Acids Res*. 2018;46(D1):D754–61. <https://doi.org/10.1093/nar/gkx1098>.
99. Zhang Y, Hoon MA, Chandrashekar J, Mueller KL, Cook B, Wu D, et al. Coding of sweet, bitter, and umami tastes: different receptor cells sharing similar signaling pathways. *Cell*. 2003;112(3):293–301. [https://doi.org/10.1016/S0092-8674\(03\)00071-0](https://doi.org/10.1016/S0092-8674(03)00071-0).
100. Zheng Y, Qin Z, Ye Q, Chen P, Wang Z, Yan Q, et al. Lactoferrin suppresses the Epstein-Barr virus-induced inflammatory response by interfering with pattern recognition of TLR2 and TLR9. *Lab Invest*. 2014;94(11):1188–99. <https://doi.org/10.1038/labinvest.2014.105>.
101. Zheng Y, Zhang W, Ye Q, Zhou Y, Xiong W, He W, et al. Inhibition of Epstein-Barr virus infection by lactoferrin. *J Innate Immun*. 2012;4(4):387–98. <https://doi.org/10.1159/000336178>.
102. Ziegler CGK, Allon SJ, Nyquist SK, Mbanjo IM, Miao VN, Tzouanas CN, et al. SARS-CoV-2 receptor ACE2 is an interferon-stimulated gene in human airway epithelial cells and is detected in specific cell subsets across tissues. *Cell*. 2020;181(5):1016–35. <https://doi.org/10.1016/j.cell.2020.04.035>.

Publisher's Note

Springer Nature remains neutral with regard to jurisdictional claims in published maps and institutional affiliations.

Ready to submit your research? Choose BMC and benefit from:

- fast, convenient online submission
- thorough peer review by experienced researchers in your field
- rapid publication on acceptance
- support for research data, including large and complex data types
- gold Open Access which fosters wider collaboration and increased citations
- maximum visibility for your research: over 100M website views per year

At BMC, research is always in progress.

Learn more biomedcentral.com/submissions

